Journal of Medicinal Chemistry

Article

Cofactor Analogues as Active Site Probes in Lysine Acetyltransferases

Roman P. Simon, Tobias Rumpf, Vaida Linkuvien#, Daumantas Matulis, Asifa Akhtar, and Manfred Jung

J. Med. Chem., **Just Accepted Manuscript** • DOI: 10.1021/acs.jmedchem.8b01887 • Publication Date (Web): 20 Feb 2019

ACS Publications

is published by the American Chemical Society. 1155 Sixteenth Street N.W., Washington, DC 20036

Cofactor Analogues as Active Site Probes in Lysine Acetyltransferases

Roman P. Simon,† Tobias Rumpf,‡ Vaida Linkuviene,§ Daumantas Matulis,§ Asifa Akhtar,‡ and Manfred Jung†,*

† Institute of Pharmaceutical Sciences, University of Freiburg, Albertstraße 25, 79104 Freiburg im Breisgau, Germany

‡ Department of Chromatin Regulation, Max-Planck-Institute of Immunobiology and Epigenetics, Stuebeweg 51, 79108 Freiburg, Germany

§ Department of Biothermodynamics and Drug Design, Institute of Biotechnology, Life Sciences Center, Vilnius University, Saulėtekio 7, 10257 Vilnius, Lithuania

ABSTRACT: Lysine acetyltransferases (KATs, also termed histone acetyltransferases, HATs) catalyze the acetylation of substrate lysine residues by employing the cofactor acetyl-coenzyme A (AcCoA), thereby providing a dynamic control mechanism of protein function. Because of their major involvement in cell development and homeostasis, small molecule modulators of KAT activity are urgently needed to assess their therapeutic potential and for probing their underlying biology. Recent advances in the field suggest that targeting the cofactor binding site represents a promising strategy for identifying potent and selective ligands. Here we present the synthesis of two functional cofactor-based chemical probes and their usage as mechanistic tools in a broadly applicable assay platform. A fluorescence polarization (FP) based binding assay was combined with biolayer interferometry (BLI) competition analysis and a FP competition activity immunoassay to enable easy, reliable, and profound evaluation of ligands that target the KAT cofactor binding site.

INTRODUCTION

The reversible acetylation of lysine residues has been identified as a means of fundamental regulation of protein and genome function, which is conserved from prokaryotes to mammals.[1-2] The dynamic acetylation equilibrium within a cell is balanced by lysine acetyltransferases (KATs) and lysine deacetylases (KDACs).[3] Although originally identified as modifiers of histone proteins (HATs and HDACs), enzymatic activity of these enzymes has also been demonstrated for a variety of non-histone substrates, underlining their important role in cell physiology.[4] All KATs employ the cofactor acetyl-coenzyme A (AcCoA (Figure 1)) to transfer an acetyl group to the ε-N moiety of lysine residues of substrate enzymes, releasing the formed acetamide and CoA. Although AcCoA is the general KAT cosubstrate, acylation activity employing other short-chain acyl-CoAs has been demonstrated for some KAT enzymes.[5-7] Based on sequence similarity and catalytic mechanism, the major KAT activity containing proteins identified in humans are grouped into three distinct families, named the GNAT (Gcn5 related N-acetyltransferase) family (including Gcn5[8], pCAF[9], HAT1[10], ATAT-1[11]), the metazoan specific p300/CBP family (including p300[12] and CBP[13]), and the MYST family (including MOF[14], MOZ, MORF[15], Tip60[16] and HBO1[17]). Multiple other enzymes have been reported to catalyze protein lysine acetylation among which are yeast homologues of mammalian KATs, non-structurally related proteins, and poorly characterized KAT candidates.[18-21] The catalytic domains of KAT enzymes share high sequence homology within a distinct family and little to no sequence similarity to other families. These core domains are generally flanked by multiple other protein modules, which directly or indirectly contribute to substrate specificity and efficacy of the acetylation reaction. The functional consequences of enzymatic lysine acetylation as a post-translational protein modification are attributable to multiple mechanisms including recruitment of acetyl lysine binding proteins, protein stabilization, autoacetylation, and chromatin relaxation.[22] Dysregulation of these processes as a consequence of KAT aberration have been causally correlated with a number of malignancy phenotypes such as neurodegenerative disease[23], viral and parasitic infections[24-25], inflammation[26], cancer[27-29], and metabolic disorders[30]. Mutations in gene sequence, changes in expression levels and fusion proteins as a consequence of chromosomal

translocation represent possible causes for dysregulated KAT activity in such diseases. Because many KATs associate with effector proteins under physiological conditions, it has been challenging to dissect whether a certain biological effect is attributable to their enzymatic activity or to their scaffolding function in a cellular context.[31] An appropriate way to encounter this problem is the use of potent and specific small molecule inhibitors to assess the biological consequences and therapeutic potential of KAT inhibition. Despite major efforts towards the identification and development of such compounds, only two drug-like inhibitors for p300/CBP[32] (KAT3a/b) and MOZ/MORF[33] (KAT6a/b), respectively, were made available until to date.[34-35] Early approaches to this topic focused on bisubstrate mimics via covalent connection of the physiological cofactor to substrate peptides (acetonyl-CoA, Lys-CoA, and H3-CoA-20; Figure 1).[36-37] While these compounds suffer from poor cell permeability and complex structure, they exhibit potent and selective KAT inhibition. The concept was adopted for the generation of functionalized chemical probes mainly for the profiling of KAT substrates and for chemoproteomic applications.[38] Selected examples are depicted in Figure 1: the reactive compound desthiobiotin-sulfone-CoA was used for active site cysteine labeling of several acetyltransferases[39], the cofactor surrogates **1a** and **1b** led to functional labeling of KAT substrates[40-41], and the bisubstrate inhibitor based probe **1c** equipped with an biotin affinity handle was used for selective enrichment of KATs from crude cell lysates.[42] In the present article, we describe our adaptation of the bisubstrate strategy to generate and characterize functionalized cofactor-based probes of reduced structural complexity to assemble a versatile and broadly applicable assay platform. The catalytic domain of pCAF (KAT2B) was used to develop a fluorescence polarization (FP)-based displacement assay supplemented with a biolayer interferometry (BLI) assay that allows for the measurement of real time binding data. Both assays were then transferred to p300 (KAT3B) and MOF (KAT8) to show the versatility of the platform. These test systems were combined with a FP competition activity immunoassay to enable easy, reliable, and profound screening, characterization, and profiling of candidate compounds that target the KAT catalytic domain.

RESULTS

Probe Design and Synthesis. Although there is a lot of data published on the inhibitory properties of cofactor analogues and bisubstrate inhibitors, comparably little is known about the thermodynamic binding affinities of respective compounds. K_D values of 0.64 ± 0.12 μM and 8.7 ± 1.2 μM have been published for AcCoA binding to pCAF and MOF, respectively.[43-44] For p300, an affinity constant of 0.74 ± 0.06 μM for the interaction with the non-hydrolyzable reference inhibitor acetonyl-CoA has been reported.[45] While it has been shown that extensive modification of the peptide part of bisubstrate inhibitors can result in better inhibitory potency and KAT specificity, we sought for a way to generate CoA analogues with a broader scope of KAT interactions to expand the applicability of these probes. We therefore conceptually reduced the peptide part to a single lysine mimicking aminohexanoic acid residue that bridges the CoA part of the probe with a functional label (Figure 2). Immobilized acetonyl-CoA has previously been used for affinity enrichment of KATs originating from different enzyme families.[46] We hypothesized that such functionally labeled CoA analogues would exhibit sufficiently high binding affinities to be used as chemical tool compounds in screening and profiling of cofactor competitive ligands. The synthesis of our probes was started with the assembly of a bifunctionalized linker, which was subsequently coupled to CoA and the functional label (Scheme 1). Therefore, Boc-protected 6-aminohexanoic acid (**2**) was condensed with propargylamine to the alkynylated intermediate **3** using standard amide bond formation. Deprotection followed by chloroacylation in DMF yielded the bifunctionalized linker **4**. We next assembled the fluorescence tag by submitting amine **5** to a 1*H*-imidazole-1-sulfonyl azide promoted diazotransfer to generate the azide **6**, which was treated with oxalyl chloride in dichloromethane in presence of catalytic amounts of DMF. The resulting acyl chloride was coupled to stoichiometric amounts of 6-aminofluorescein to yield the fluorescence tag **7**. Finally, alkyl linker **4** was converted to the respective probes. For the fluorescence labeled derivative, **4** and **7** were combined in a Cu-catalyzed Huisgen cycloaddition to furnish compound **8**, which was further reacted with CoA in a S_N2 reaction to generate the probe **11**. In the case of the affinity labeled probe, nucleophilic substitution of the alkyl halide was carried out first (**9**), followed by the cycloaddition reaction to yield the

desired compound **12** (Figure 2). In the next step, we selected pCAF as a prototypical KAT for probe validation and assay development, because of its high cofactor binding affinity and well-defined binding mode. The catalytic domain of pCAF fused to a N-terminal His-tag (pCAF(493-658) was expressed and purified from *E. coli* cells to provide sufficient amounts of protein. To test whether our compounds are capable to bind to the investigated KAT proteins, a pull-down experiment was carried out. Streptavidin coated magnetic beads were used in combination with **12** to individually capture recombinant proteins from solutions in the presence of BSA (Supporting Information, Figure S1). Control experiments containing either 100 μM acetonyl-CoA or 50 μM biotin were included for every KAT. SDS-gel analysis of the isolated fractions showed successful pull-down of all three KAT proteins respectively, which is indicative for effective binding of **12** to the tested enzymes. Next, we aimed at quantifying the binding affinities of the probes. ITC measurements of pCAF(493-658) interacting with either the physiological cofactor AcCoA, the reference inhibitor acetonyl-CoA, fluorescence labeled probe **11**, or the affinity labeled probe **12**, yielded K_D values of 0.77 ± 0.17 μM, 0.71 ± 0.31 μM, 0.75 ± 0.36 μM, and 1.39 ± 0.23 μM, respectively (Supporting Information, Figure S2). These results are in good agreement with the previously published binding affinity for AcCoA (0.64 ± 0.12 μM) and demonstrate the possibility to functionally label at the selected derivatization site whilst maintaining binding affinities comparable to the physiological ligand. With the probes **11** and **12** validated as efficient binders of three different KAT proteins, we then turned our attention to the applications of the tool compounds.

Fluorescence Polarization Competition Assay. The labelled CoA analogue **11** was used as a fluorescent tracer to set up a competition binding fluorescence polarization assay. As the degree of polarization is inversely proportional to the molecular mobility and therefore correlates with the size of the fluorescent species, the polarization signal increases with the fraction of **11** bound to the receptor (here KAT protein). In a setup with fixed concentrations of **11** and KAT protein, competing test ligands reduce the fraction of tracer that is bound to the receptor, which results in a decrease of measured mP values (Figure 3a). To assess the optimal probe concentration, we prepared a serial dilution of **11** in assay buffer covering a

concentration range of 3.8-30 nM in 20 µl volume and measured the fluorescence intensities (FI) in the p- and s-plane. Resulting values were plotted against probe concentrations to show a linear increase of fluorescence intensity for both planes (R^2=0.999 and 0.999) and a stable ratio of FI values over the entire concentration range (Supporting Information, Figure S3a). A probe concentration of 8 nM was selected for further experiments as this amount of **11** gave FI values that exceeded the values measured for buffer controls five times, which resulted in a stable and robust FP signal. We next performed a saturation binding experiment by titrating a dilution series of pCAF(493-658) protein to **11** in presence or without a saturating concentration of reference inhibitor (200 µM acetonyl-CoA). To control for intrinsic protein fluorescence, the protein dilution series was also incubated without fluorescent tracer. The fluorescence intensities for p-plane and s-plane were then measured from all wells and values from the protein fluorescence controls were subtracted from tracer containing wells for every pCAF(493-658) protein concentration. From the resulting fluorescence intensities, the mP values were calculated. From reference inhibitor containing wells, the non-specific portion of measured fluorescence polarization signals was determined and values were corrected accordingly. With the resulting signals for specific binding of **11** to pCAF(493-658) we were able to calculate the affinity constant of the interaction, which was determined to be K_D = 824 ± 40 nM by non-linear regression using a one-site binding fit (Figure 3b). This value is in excellent agreement with our results from ITC measurements and sufficiently low to use **11** as a fluorescent tracer in FP applications. Further, by calculating total fluorescence intensities, we were able to show that there is no substantial fluorescence quenching event evident upon binding of tracer to the protein (Supporting Information, Figure S3b). To test the competitive displacement of **11** from binding to pCAF(493-658), we then titrated acetonyl-CoA to mixtures containing fixed concentrations of protein and tracer (400 nM and 8 nM, respectively) and measured the FP signal at different time points. The relative competition compared to control wells was calculated for every ligand concentration and resulting values were plotted against acetonyl-CoA concentrations. Figure 3b shows the results from this experiment after non-linear curve fitting, demonstrating a stable dose-response at all measured time-points. From obtained IC_{50} values, an affinity constant for the interaction of acetonyl-CoA to pCAF(493-658) of K_D = 592 ± 66

nM was calculated, which again is in good agreement with the value determined by ITC. With optimized assay parameters of 400 nM pCAF(493-658), 8 nM **11**, and 30 minutes incubation time, we investigated the influence of increasing DMSO content on our system. Therefore, we measured positive controls, containing all assay components and increasing amounts of DMSO (v/v), and compared them to negative controls containing 50 µM acetonyl-CoA additionally (Supporting Information, Figure S3c). The signal window of the assay did not decrease by more than 10% for concentrations up to 8% (v/v) of organic solvent. We selected a standard DMSO concentration of 5% (v/v) for the screening of ligands targeting the CoA binding site and evaluated the reproducibility and robustness of the assay by preparing 32 positive and 32 negative (containing 50 µM acetonyl-CoA) controls on a single 384-well plate. From the FP signals of these measurements, the Z'-factor for the assay was calculated as described by Zhang et al. as a surrogate for assay quality (Supporting Information, Figure S3d).[47] With a Z'-factor of 0.81 our assay meets the requirements for a stable and robust assay (Z' > 0.5) and facilitates the screening for competitive ligands targeting the cofactor binding site.

Biolayer Interferometry Binding Assay. As a confirmatory biophysical assay, we chose biolayer interferometry as a method to revalidate candidate ligands identified as competitors by the fluorescence polarization competition assay. BLI measures the interference pattern of white light that is reflected on a biocompatible surface immobilized on a sensor tip compared to a reference beam. Upon binding of biomolecules to the functionalized surface the optical thickness of this layer increases, which results in a shift of the interference pattern that is expressed in nm. The increase of the BLI signal is proportional to the number of biomolecules bound to the functionalized surface and can be measured in real time proving a means for the determination of kinetic data of the molecular interaction. In our approach, we used streptavidin coated sensor tips to immobilize the biotinylated CoA analogue **12** onto the biosurface and investigate the binding of acetyltransferase protein to the immobilized probe (Figure 3c). First, we determined the optimal loading density of **12** on the biosensors. Oversaturation of biosensors can cause steric hindrance and aggregation, whereas too little ligand immobilized can result in insufficient signal

intensities. To assess a suitable loading concentration, a dilution series of **12** in assay buffer was prepared and the BLI signal increase during the loading step and subsequently for the binding phase, during which the loaded sensors were exposed to a 1 μM solution of pCAF(493-658), were monitored (Supporting Information, Figure S4a and S4b). A probe concentration of 125 nM was found to give a linear signal increase in the loading phase without reaching saturation while the signal increase during the binding phase remained sufficiently high. Next we decided to measure a K_D value for the interaction of pCAF(493-658) to immobilized **12**. Because global fitting of sensorgrams to a one site binding model for different protein concentrations was unprecise in the dissociation phase, we decided to use a saturation binding approach for the determination of the affinity constant (Supporting Information, Figure S4c). Therefore, we incubated preloaded biosensors with a dilution series of protein concentrations spanning from 0.04 μM to 30 μM, which was supposed to cover a concentration range of approximately 0.05 to 20 times K_D. Exposure of a biotin blocked biosensor to 30 μM pCAF(493-658) in assay buffer showed no significant increase in binding signal, suggesting the absence of unspecific interactions of the protein to the biosensor. BLI signals for the association- and dissociation phase were recorded as described in the experimental section (Figure 3d). Report points at the end of the association phase were then used to extract binding signals from the recorded sensorgrams for every protein concentration used. Plotting of these values against protein concentration followed by non-linear curve fitting to a one site binding model gave a K_D value of 1.00 ± 0.28 μM, which is in good agreement with values determined by ITC and FP (1.39 ± 0.23 μM and 0.71 ± 0.08 μM, respectively). To test the feasibility of the system to evaluate compounds as competitive ligands, we tested the influence of increasing concentrations of reference inhibitor in protein solutions on the sensorgrams of the association step. A fixed concentration of 250 nM pCAF(493-658) was incubated with different amounts of acetonyl-CoA and the association curves were recorded on the BLI instrument (Figure 3e). We observed a concentration dependent decrease in binding signal with a maximum that almost reached blank (loaded sensors in assay buffer) level. Comparing the BLI signals at report points set at the end of the association phase allowed us to quantify the degree of competition for every acetonyl-CoA concentration and plotting of respective nm values against ligand

concentrations gave an IC_{50} value of 0.78 ± 0.10 μM (Figure 3e). This value is very close to the K_D values for the interaction of pCAF(493-658) with acetonyl-CoA determined by other methods and shows the utility of the assay for the validation of candidate ligands.

Applicability of the Assays to Other Family KATs. To test the applicability of the FP assay and the BLI assay to other KAT family members, we chose two representative KATs, p300 (p300(1284-1673)) of the p300/CBP family and MOF (MOF(174-449)) of the MYST family, and subjected them to the same cycles of assay optimization as described for pCAF (Figure 4). For p300(1284-1673), slow but tight binding to the fluorescent probe was observed and in comparison to pCAF, longer incubation times were needed to reach equilibrium. The FP saturation binding experiment yielded a K_D value of 396 ± 31 nM for binding to **11**, which allowed to calculate an affinity constant of K_D = 653 ± 56 nM for the reference inhibitor from the dose-response curve. This value is close to the published value of 780 ± 60 nM. The slow binding of p300(1284-1673) was also observable in the BLI assay and the protocol had to be adjusted accordingly. Instead of loading the biosensor with **12** first, we incubated the protein with 125 nM probe alone or in the presence of competing ligands for 30 minutes and measured the association to the streptavidin coated sensor from these solutions. While this does not allow for deducing any kinetic data from the association curves, the new protocol proved to be usable to evaluate ligands competitive to **12**. Titrating acetonyl-CoA in this assay resulted in an IC_{50} of 779 ± 30 nM. Notably, the tight binding of p300(1284-1673) to **12** was reflected in only very little dissociation of the protein from the sensortip during the dissociation step (k_{off} = $2.1 \cdot 10^{-4}$ $1 \cdot s^{-1}$). For MOF(174-449), the saturation binding experiment yielded a K_D value of 1.39 ± 0.11 μM for binding to **11**. The increase in FP signal in this experiment was less pronounced compared to the other tested KAT proteins. The affinity constant for MOF(174-449) binding to acetonyl-CoA was determined from this experiment and resulted in K_D = 1.58 ± 0.14 μM, which is distinctly lower than the published value for the protein cofactor interaction (8.7 ± 1.2 μM). Since we were not able to measure BLI signals at sufficiently high protein concentrations to reach saturation binding, we determined a K_D = 4.13 ± 0.4 μM for MOF(174-449) binding to **12** by applying a global one site binding fit to the sensorgrams of a protein dilution series (Supporting Information, Figure S4d). Titrating the reference inhibitor against 4

μM protein in this assay resulted in an IC_{50} of 1.35 ± 0.18 μM for acetonyl-CoA. Together, these experiments demonstrate the broad applicability of **11** and **12** as chemical tool compounds for KAT enzymes and the versatility of our assays platform.

FP Competition Activity Immunoassay. To complement the biophysical test systems, we sought for a non-radioactive assay to measure the activity of the investigated acetyltransferases under *in vitro* conditions. We also aimed at an approach that does not require the use of labeled substrates or reactive detection reagents, which can lead to data artefacts like high background signals or false positive screening hits. Because of our good experience with fluorescence polarization, we hypothesized that it would be possible to design an assay that measures the enzyme activity dependent competition of reaction product to a fluorescence labelled tracer for binding to a specific antibody, as it has been reported for kinases (Scheme 2).[48] This would allow for free scaling of substrate and cofactor concentrations and the use of unlabeled and more physiological peptide or protein substrates. Although the preferred H3 acetylation site for pCAF has been reported to be H3K14, we had obtained good signal to background ratios using a polyclonal anti-acH3K9 antibody (#39137, Active Motif) in our biochemical assays (data not shown). As a fluorescent tracer, we used a peptide that contains the first 14 amino acids of the histone H3 N-terminal sequence with a rhodamine label attached to the side chain of K 14 and an acetylated K9 moiety (acH3K9-Rh). For MOF(174-449) and p300(1284-1673), we expected a broader spectrum of acetylation products. Therefore, a tetra-acetylated H4(1-23) peptide with a C-terminal fluorescein label was used as a tracer (acH4-Fl). The exact sequence of peptides can be found in the Supporting Information. The fluorescent properties of acH3K9-Rh and acH4-Fl were investigated as described for **11** and tracer concentrations of 8 nM and 3 nM were selected, respectively (Supporting Information, Figure S5a). In the next step, different antibodies were titrated to solutions containing the indicated concentration of acH3K9-Rh or acH4-Fl and 10 μM of H3(1-21) peptide or H4(1-23) peptide, respectively, in 25 μl volume on 384-well microtiter plates and the changes in FP signals were recorded. Satisfactorily, we identified two antibodies that were capable to bind their epitope in solution thereby inducing a

concentration dependent FP signal increase (Figure 5a). Our selected anti-acH3K9 antibody caused an almost linear increase in mP values up to the highest concentration tested (5 µg/ml), which corresponds to a 1:200 dilution in a final assay volume of 25 µl. For acH4-Fl, the only antibody with a good response in this experiment was a monoclonal anti-acH4 antibody (#177790, abcam) directed against tetra-acetylated H4 (K5, 8, 12, 16). Addition of anti-acH4 to the tracer peptide resulted in a steep increase of FP signal that leveled around 160 mP for antibody concentrations exceeding 0.5 µg/ml (1:700 in 25 µl volume). The feasibility of the setup to measure KAT activity was then investigated for established tracer/receptor pares (8 nM acH3K9-Rh/5 µg/ml anti-acH3K9 and 3 nM acH4-Fl/0.4 µg/ml anti-acH4, respectively). For successful activity measurements, the product of the enzymatic reaction has to be competitive to the tracer peptide for binding to the antibody. If the system fulfills this requirement, the degree of competition can be calculated from recorded FP values and is proportional to enzyme activity. Concentration series of enzymes were incubated with substrate peptide or protein (50 µM H3(1-21) for pCAF(493-658), 5 µM full length H4-His for MOF(174-449) and 5 µM H4(1-23) for p300(1284-1673)) and 20 µM AcCoA for 60 minutes. Enzymatic reactions were then stopped by adding 2.5 µl of tracer solution containing 500 µM acetonyl-CoA followed by a short incubation step. Finally, 2.5 µl antibody solution in assay buffer were dispensed into every well and after an additional 30 minutes incubation step, FP signals were recorded and competition values calculated. Figure 5b shows a clear increase in competition with increasing enzyme concentrations, which strongly suggests a concentration dependent displacement of tracer from the receptor by the product of enzymatic turnover. Further, the use of full length H4 histone protein as a substrate demonstrates the capability of the assay to use physiological protein substrates. Enzyme concentrations from the ends of the linear portions of the enzyme progression curves were selected for further experiments (30 nM pCAF(493-658), 50 nM MOF(174-449), and 15 nM p300(1284-1673)). We then determined the assay specific K_m values for AcCoA and selected screening concentrations that, again, were at the upper end of the linear portion of the Michaelis-Menten plots to preserve a sufficient assay window (Supporting Information, Figure S5b). With the defined assay parameters, dose-response curves for the reference inhibitor were recorded (Supporting Information, Figure S5c) and K_i values were

calculated according to the method of Cheng and Prusoff.[49] We also determined the assay specific Z'-factors (all > 0.5) as a measure of assay robustness (Supporting Information, Figure S5d). The exact results from our activity assay development and reference inhibitor validation are summarized in Table 2.

Versatility of the Assay Platform. With the evaluated tool compounds and optimized assay parameters, the utility of the assay platform for different applications was investigated.

Profiling of acyl-CoA variants: First, we followed observations by Montgomery et al. [42] and Ringel et al.[50] who have reported inhibitory properties of metabolic acyl-CoAs (e.g. butyryl-CoA and several long-chain acyl-CoAs(Figure 1)) on the GNAT family KAT hGcn5. To validate the role of the chain length and quantify the degree of interaction, a small set of acyl-CoA cofactor analogues were profiled for their binding properties to the closely related Gcn5 homologue pCAF. We included the enzymatic reaction product CoA (C-0), the physiological cofactor AcCoA (C-2), butyryl-CoA (C-4), lauroyl-CoA (C-12), aromatic benzoyl-CoA, and the more hydrophilic acyl-CoA variant hydroxybutyryl-CoA. A comparison of the competition profiles from FP and BLI assays showed a strong increase of interaction for the physiological cofactor compared to the enzymatic reaction product CoA (Figure 6a). Elongation of the carbon chain to a butyryl residue then resulted in a drop of competition to CoA level. The same effect was observed for structurally more demanding acyl-CoA variants benzoyl-CoA and hydroxybutyryl-CoA. Further elongation to the C-12 derivative lauroyl-CoA then led to a strong increase of potency that exceeded the level of AcCoA. Recording the dose-response curves of acyl-CoA variants with increasing chain length in the FP assay allowed us to calculate the affinity constants of respective interactions from IC_{50} values (Figure 6c). We then revalidated our findings by comparing the results from FP and BLI assays to the stabilizing effects (ΔTm**)** of tested CoA analogues in a fluorescent thermal stability assay (Figure 6b). Table 3 shows the results from these experiments and assigns lauroyl-CoA as a potent binder ($K_D = 0.18 \pm 0.01$ μM) of pCAF(493-658) with a five times higher affinity than the physiological cofactor ($K_D = 1.03 \pm 0.09$ μM). To test whether the high affinity also translates to inhibitory potency, lauroyl-CoA was evaluated in the FP competition activity immunoassay (Figure 6d). The compound inhibits

pCAF(493-658) more potently (K_i = 0.78 ± 0.18 μM) than the reference inhibitor acetonyl-CoA (K_i = 1.32 ± 0.24 μM). Molecular docking to hGcn5 and crystallographic data of p300 has shown that the alkyl chain of CoA variants is positioned in the lysine binding site of the enzymes.[42, 45] Structural analysis of p300 further revealed the presence of a hydrophobic binding pocket located at the catalytic center of the protein, a structural feature absent in pCAF and MOF. This pocket was proposed to accommodate the alkyl portion of structurally more demanding acyl-CoAs after substrate induced ligand rearrangement during the catalysis of the acyl transfer by p300.[45] To compare the effects of acyl-CoAs on pCAF(493-658) with effects on p300(1284-1673), the ability of both enzymes to use acyl-CoA variants as cofactor for enzymatic turnover of a peptide substrate was tested in a thiol scavenging assay that detects the acyl-CoA hydrolysis product CoA (Supporting Information, Figure S6a). As expected, p300, but not pCAF, is capable to use butyryl-CoA and hydroxybutyryl-CoA for enzymatic turnover, although the efficiency of turnover is decreased compared to AcCoA. In the presence of lauroyl-CoA, no activity could be detected within this assay. The profile of acyl-CoAs in the FP assay was then recorded for p300(1284-1673). Interestingly, in contrast to pCAF, the degree of competition for binding to p300 did not show an initial decrease with increasing chain length but increased continuously from C-2 to C-12 (Supporting Information, Figure S6b). Dose-response analysis revealed that, despite being less effective cofactors, p300(1284-1673) binds butyryl-CoA and lauroyl-CoA with significantly higher affinities than the predominant cofactor AcCoA (Figure 6c). This observation is in agreement with inhibition data from the FP competition activity immunoassay (Figure 6d). We then tested whether the increased affinity of lauroyl-CoA could be attributable to additional interactions of the ligand with the peptide binding site of the enzymes. Therefore, a peptide binding assay (Alpha) was performed, which showed considerable competition of lauroyl-CoA, but not of the reference inhibitor or probe **11**, for binding of His-tagged pCAF to biotinylated H3(1-21) peptide (Supporting Information, Figure S6c). Together, our results propose that the comparatively high affinity of lauroyl-CoA for pCAF(493-658) and p300(1284-1673) is the result of additional hydrophobic interactions of the ligand with the substrate binding site of the respective protein. In the case of pCAF, this site seems to be located distally to the lysine binding groove

where the N- and C-terminal regions have been shown to form strong van der Waals contacts with the physiological substrates.

Probing the cofactor binding site: We were interested in the possibility of using **11** to identify structural features of the cofactor that are crucial for binding to the respective KAT enzyme. A comparison of such features for all our tested KATs could possibly reveal differences in protein cofactor interactions, which could prove useful in the design of more specific ligands targeting the CoA binding site. To do so, a set of chemical entities containing different structural motifs of the cofactor was assembled and each compound was tested at a fixed concentration of 1 mM against every KAT in the FP assay (Figure 6e). By this, we were also able to validate the assay for its applicability to fragment-based approaches. The results from this experiment are depicted in Figure 6. The strong interaction of CoA´s phosphate backbone with the cofactor binding site has previously been shown for pCAF[51], p300[52], and MOF[53] by crystallographic means and our findings accordingly show a pronounced decrease in competition for fragments lacking one or more phosphate moieties. For all tested KATs, the segmentation of the cofactor into two individual fragment portions, the pantetheine part and the adenosine phosphate part, led to an almost complete loss of interaction. Only the adenosine 3',5'-diphosphate fragment exhibited modest competition with the probe for binding to KAT proteins. For MOF, competition exceeding 20% was also observed for ADP, which was completely inactive against pCAF and p300. Unphosphorylated pantethein did not exhibit any significant competitive displacement of the fluorescent tracer, as it was proposed based on the findings of previous studies on the interaction of pantethein analogues with acetyltransferases.[54-55] A comparison of competition values for the three KAT enzymes shows an overall better amenability of MOF to CoA-fragment competition, which likely is due to the comparatively lower affinity of MOF(174-449) to **11**. In the case of p300(1284-1673), a strong effect on binding was observable for the 3'-phosphate residue, as the cofactor fragment lacking only this moiety (dephospho-CoA) was not able to promote full competition to **11**, even at a concentration as high as 1 mM (CoA FP-assay IC_{50} = 3.0 ± 0.2 μM). Together, our comparison of fragment competition enables an interaction mapping of the cofactor binding site that is in good accordance with findings from structural biology approaches. These results suggest that the tested

KAT enzymes share a strong dependence of binding potency on the presence and precise orientation of phosphate residues within the cofactor structure. Still, differences in the overall competition profile of cofactor fragments between the different KAT enzymes could be observed in our FP approach, demonstrating the applicability and versatility of **11** for this method.

Fragment-based ligand screening: To show the feasibility of the assay platform to screen larger quantities of candidate ligands for binding to KAT protein, we performed a fragment-based approach. 1000 small molecule fragments from a commercially available library (rule of 3 compliant) were evaluated in the FP assay against pCAF(493-658). Compounds were first screened at 1 mM in duplicates and a statistic cut-off of two times the mean standard deviation over all measurement was applied (Figure 7a). In a second round, 62 initial hits were tested at three different concentrations (3 mM, 1 mM, and 0.3 mM). Fragments that gave at least 30% inhibition at 3 mM and a two-fold increase in inhibition over the concentration range were considered as hits. Autofluorescent compounds were discarded. The remaining 27 compounds were then subjected to a fluorescent thermal stability assay and destabilizing fragments ($\Delta T_m < -1$ °C) were sorted out (Figure 7b). Eventually, 14 fragments that showed a good response in the FP assay and no protein destabilizing effects were evaluated for their competitive effects at 1 mM in the BLI assay (Figure 7c). Three fragments prevented binding of pCAF in this assay by more than 20% and their structures are depicted in Figure 7d. These fragments share the structural motif of a five- or six-membered aromatic heterocycle with a carboxylic acid residue in position 2, which indicates that we successfully enriched a certain chemotype that showed effective competition to our probes for binding to the cofactor binding site of pCAF(493-658) in two orthogonal assay systems.

DISCUSSION AND CONCLUSION

In the present study, we report the development of two cofactor-based chemical tool compounds, fluorescently labeled compound **11** and biotin labeled compound **12,** and their utilization in development of a biophysical assay platform for the evaluation of candidate ligands targeting the KAT cofactor binding site. The structures of these probes were deduced from the bisubstrate concept of covalently linking the products of enzymatic turnover, CoA and an acetylated lysine mimic, via a non-hydrolysable thioether linkage. By reducing the substrate mimicking moiety to a simple aminohexanoic acid residue and coupling of the functional label to this site, the resulting compounds exhibit a broad applicability across KAT enzymes originating from different enzyme families, while maintaining sufficiently high binding affinities to be used in binding assays. While such tool compounds lack the cell permeability and selectivity to be used in biological systems they provide a valuable means for *in vitro* evaluations. Recent reports of the first potent and selective small molecule inhibitors of p300/CBP[32] and MOZ/MORF[33] activity, both targeting the cofactor binging site of the respective enzyme, underline the potential of our cofactor competition binding approach. The target compounds were synthesized via a convergent route with an intermediate clickable handle that enables easy functionalization with a label of choice. We used the fluorescence labeled probe **11** to set up a FP-based competition assay for the evaluation of active site ligands. The relative increase in molecular volume upon binding and the conformational constraint of the fluorophore are the main drivers for the generation of a sufficient dynamic assay window. While larger peptide-based bisubstrate ligands could provide higher affinity and subtype selectivity, they are limited by their structural flexibility at possible label attachment sites and high molecular weights. The comparatively smaller size of **11** and the labelling in a position that places the fluorophore close to the lysine binding site facilitated its use as a tracer in FP applications with sufficient signal intensities. After successful implementation of the FP-assay, we optimized assay parameters for representative KAT enzymes from each of the three major families The same was achieved with the affinity labeled cofactor derivative **12** in a BLI-based setup. Utilizing the reference inhibitor acetonyl-CoA, these assays were then used to record thermodynamic and kinetic binding data, which is in excellent agreement with previously

published values and data from ITC measurements, thus validating our probes and assays as sensitive and versatile tools for the identification and characterization of cofactor competitive ligands. The combination of binding assays with a system that measures enzyme activity provides an orthogonal means to assess the functional consequences of cofactor competition by candidate ligands. For this approach, we reported a non-radioactive FP competition activity immunoassay that does not rely on substrate labels, reactive detection reagents, or functional surfaces, but allows free scaling of substrate and cofactor concentrations and the use of whole protein substrates, which resemble a more physiological background. Although such assay formats have been reported for kinases, to our knowledge, this is the first report of a FP competition immunoassay measuring KAT activity to date. The application of the entire assay platform was further validated by three different approaches. First, profiling of acyl-CoA variants revealed distinct binding affinity patterns dependent on the alkyl chain length of the acyl moiety for pCAF and p300. The potent binding of lauroyl-CoA to these enzymes was also shown to translate into inhibitory potency and for pCAF we were able to rationalize our findings by demonstrating competition of the long chain acyl-CoA to the peptide substrate, suggesting additional interactions with the protein at the substrate binding site. Further, we used cofactor fragments to identify critical interaction sites and systematically tested structural motifs of the physiological ligand to reveal subtype selective characteristics. **11** and **12** were finally used to screen a commercially available fragment library in consecutive screening steps and we identified three structurally analogous compounds that show profound and dose-dependent competition to the probes for binding to pCAF, whilst not showing any disruption of protein integrity or assay interference. Such screening hits provide excellent candidates for future cocrystallization and crystal soaking experiments to develop the initial hits into new lead-like candidates by structure guided medicinal chemistry approaches.[56] Since the here reported tool compounds are likely promiscuous to other CoA utilizing enzymes, our biophysical approach is presumably transferable to other *in vitro* setups. In summary, we propose that our probes and assays are versatile and valuable tools for the *in vitro* evalutation of KAT characteristics, which will prove useful for the identification and profiling of new drug candidates targeting the cofactor binding site.

EXPERIMENTAL SECTION

General: Starting materials (chemicals) were purchased from commercial suppliers and used without any further purification. Solvents were used in p.a. quality and dried according to common procedures, if necessary. Thin-layer chromatography (TLC) for reaction monitoring was performed with alumina plates coated with Merck silica gel 60 F254 (layer thickness: 0.2 mm) or Merck silica gel 60 RP-18 F254 (layer thickness: 0.2 mm) and analyzed under UV-light (254 nm). Flash column chromatography was performed with TELOS Flash-LL Silica Columns 60M (0.040-0.063 mm, 230-400 mesh) as a stationary phase on a Biotage Isolera One automated flash purification system with UV-Vis detector. Size exclusion chromatography of compounds was conducted using Sephadex-G10 media and dest. H_2O as the eluent. All yields were not optimized. NMR spectra were recorded using a Bruker Avance III HD Spectrometer (1H: 400 MHz, 13C: 100 MHz) instrument. The spectra are referenced against the NMR solvent and are reported as follows: chemical shift δ (ppm), integration, multiplicity (s = singlet, d = doublet, dd = doublet of doublets, t = triplet, q = quartet, p = quintet, m = multiplet), coupling constant (J in Hz), and assignment. Mass spectra were recorded on a LCQ Advantage or Exactive device (Thermo Fisher Scientific, Waltham, MA) or an Expression CMS device (Advion, Ithaca, NY). Purity was determined by HPLC analysis using an Agilent 1260 Infinity series system with a Synergi Kinetex XB-C18 100 Å, 250 x 4.6 mm as the analytical column and UV detection (λ = 210 nm (HPLC-Method A) or 260 nm (HPLC-Method B). A linear gradient of eluent A (water + 0.05 % (v/v) TFA) and eluent B (ACN + 0.05 % (v/v) TFA) of 0–4 min, A=90%, B=10%; 4–29 min, linear increase to B=100%; 29–31 min, B=100%, 31–40 min A=90%, B=10% was applied at a constant flow rate of 1 $ml \cdot min^{-1}$. All synthesized compounds were found to possess purities ≥ 95% by HPLC analysis. Peptides were purchased from PSL GmbH, Heidelberg, Germany. p300(1284-1673) enzyme was purchased from Enzo Life Science, Farmingdale, USA.

PAINS analysis: Active compounds were tested for known classes of assay interference compounds with the publicly available online tool "False Positive Remover" (www.cbligand.org). None of the tested compounds were flagged as PAINS. In addition, all compounds reported in this study were characterized

in at least two individual assays with different readout techniques to provide orthogonal prove of their specific activities.

Chemistry:

Method A: General procedure for the Cu-catalyzed Huisgen cycloaddition: Alkyne (1 equiv.) and azide (1.1 equiv.) were dissolved in a water/*tert*-butanol mixture (2 ml, 1:1). TBTA (0.1 equiv.) was dissolved in 1 ml DMF and added to the reaction mixture. An aqueous $CuSO_4$ solution (0.1 M, 0.1 equiv.) and an aqueous solution of sodium ascorbate (0.1 M, 0.2 equiv.) were added in that order. The resulting reaction mixture was stirred for 12 h at room temperature under nitrogen atmosphere. After completion, the reaction was quenched by the addition of 5 ml of H_2O and the aqueous phase was extracted with ethyl acetate (3x 15 ml). The product containing layer was collected and solvents were evaporated under reduced pressure. The crude product was purified using automated column chromatography or semi preparative HPLC.

Method B: General procedure for the nucleophilic halide substitution: To a solution of CoA trilithium salt (1 eq.) in 0.1 M TEAB buffer pH 8.5/EtOH (4 ml, 1:1) at 0 °C was added dropwise chloroacetone (1.2 equiv.) in 2 ml EtOH. The solution was stirred under nitrogen atmosphere at 0 °C for 2 h and then allowed to warm to room temperature and stirred overnight. The reaction was quenched by the addition of 10 ml H_2O and the aqueous phase was washed with ethyl acetate (3x 20 ml). The aqueous layer was separated and solvents were evaporated under reduced pressure. The crude product was then purified using semi preparative HPLC.

acetonyl-CoA: Method B using CoA trilithium salt (300 mg, 0.37 mmol) and chloroacetone (35 µl, 0.44 mmol). 255 mg (0.4 equiv. TEA), 80 % yield; ^{1}H NMR (400 MHz, D_2O) δ 8.65 (1H, s, H-17), 8.43 (1H, s, H-20), 6.21 (1H, d, *J* = 5.4 Hz, H-16), 4.89 (2H, d, *J* = 5.3 Hz, H-14 and H-15), 4.60 (1H, s, H-13), 4.26 (2H, s, H-12), 4.01 (1H, s, H-7), 3.86 (1H, dd, *J* = 9.5, 4.9 Hz, H-11), 3.61 (1H, dd, *J* = 10.0, 4.9 Hz, H-11), 3.52 (2H, s, CO-C*H*$_2$-S), 3.46 (2H, t, *J* = 6.6 Hz, H-5), 3.31 (2H, t, *J* = 6.6 Hz, H-2), 2.60 (2H, t, *J* = 6.6 Hz, H-1), 2.46 (2H, t, *J* = 6.5 Hz, H-4), 2.28 (3H, s, C*H*$_3$-CO), 0.94 (3H, d, *J* = 7.7 Hz, H-9 or 10), 0.81 (3H, s, H-9 or 10). HPLC purity (HPLC-Method A): 97.5% (t_R = 4.72 min.);HRMS (ESI$^-$): m/z calc.

for $C_{24}H_{40}N_7O_{17}P_3S$ $[M-H]^-$ = 822.1341; $[M+Li-2H]^-$ = 828.0678; found: $[M-H]^-$ = 822.1332; $[M+Li-2H]^-$ = 828.1414

tert-butyl(6-oxo-6-(prop-2-yn-1-ylamino)hexyl)carbamate (3): 6-*tert*-butylaminocaproic acid (2) (2.169 g; 9.28 mmol) and HBTU (3.520 g, 9.28 mmol) were mixed in 50 ml dichloromethane and DIPEA (4.85 ml, 27.8 mmol) was added. After stirring for 5 minutes, propargylamine (646 µl, 9.38 mmol) was added dropwise to the mixture. The reaction was stirred overnight and the organic phase was washed with saturated $NaHCO_3$ solution, 1 M HCl and brine (3x 50 ml, each). The organic layer was then dried over Na_2SO_4 and the solvent was removed by evaporation. Purification of the crude material was achieved by automated column chromatography (cyclohexane/ ethyl acetate, 20-100 %) to obtain compound **5** as a white solid. 1.668 g, 67 % yield; ^{1}H NMR (400 MHz, methanol-d_4): δ 3.94 (2H, d, *J* = 2.6 Hz, NH-C*H*$_2$-C≡CH), 3.02 (2H, t, *J* = 7.0 Hz, H-6'), 2.57 (1H, t, *J* = 2.6 Hz, C≡C*H*), 2.19 (2H, t, *J* = 7.5 Hz, H-2'), 1.62 (2H, p, *J* = 7.5 Hz, H-5'), 1.52 – 1.45 (2H, m, H-3'), 1.43 (9H, s, (C(C*H*$_3$)$_3$), 1.37 – 1.28 (2H, m, H-4'). MS (ESI+): m/z calc. for $C_{14}H_{24}N_2O_3$ $[M+Na]^+$ = 291.2; found $[M+Na]^+$ = 291.4.

6-(2-chloroacetamido)-N-(prop-2-yn-1-yl)hexanamide (4): The Boc-group of propargylation product **3** (1.208 g, 4.50 mmol) was cleaved by addition of 15 ml TFA/dichloromethane and stirring for 2 hours. Solvents were then evaporated and remaining TFA was coevaporated with methanol (5x). The residue was then dissolved in 11 ml DMF and DIPEA (3.91 ml, 22.5 mmol) was added to the solution. After stirring for 10 minutes, the mixture was cooled to 0 °C and chloroacetyl chloride (717 µl, 9.01 mmol) in 2 ml DMF was added dropwise over a period of 30 minutes. The reaction was quenched after 2 hours by adding 50 ml of saturated $NaHCO_3$ solution. Crude product **4** was extracted from the aqueous phase with DCM (3x 50 ml) and the organic layers were combined and dried over Na_2SO_4 to give a black solid after evaporation of the solvent. The residue was purified by means of column chromatography using a gradient of methanol in dichloromethane (3-12 %). Product **4** was isolated as an off-white solid. 0.848 g, 77 % yield; ^{1}H NMR (400 MHz, methanol-d_4): δ 4.02 (2H, s, NHCO-C*H*$_2$-Cl), 3.94 (2H, d, *J* = 2.6 Hz, NH-C*H*$_2$-C≡CH), 3.22 (2H, t, *J* = 7.1 Hz, H-6'), 2.57 (1H, t, *J* = 2.6 Hz, C≡C*H*), 2.20 (2H, t, *J* = 7.5 Hz, H-2'),

1.63 (2H, p, *J* = 15.2, 7.5 Hz, H-5'), 1.54 (2H, p, *J* = 7.5 Hz, H-3'), 1.40 – 1.30 (2H, m, H-4'). MS (ESI+): m/z calc. for $C_{11}H_{17}ClN_2O_2$ $[M+Na]^+$ = 267.1; found $[M+Na]^+$ = 267.0.

4-azidobutanoic acid (6): γ-aminobutanoic acid (**5**) (1.050 g, 10.18 mmol), imidazole-1-sulfonylazide * HCl (2.565 g, 12.26 mmol), potassium carbonate (2.084 g, 15.08 mmol) and copper sulfate * 5 H_2O (29.3 mg, 0.12 mmol) were dissolved in methanol and stirred overnight under nitrogen atmosphere. The solvent was then removed by evaporation and the residue was taken up in demin. H_2O and acidified to pH 2 using HCl (5 M). The resulting suspension was extracted with ethyl acetate (3x 100 ml) and the organic layers were combined and dried over Na_2SO_4. After removing the organic solvent by evaporation, the resulting crude material was purified by automated column chromatography using a gradient of 1-5 % methanol in dichloromethane to yield product **6** as colorless oil. 1.135 g, 86 % yield; ^{1}H NMR (400 MHz, methanol-d_4): δ 3.36 (2H, t, *J* = 6.8 Hz, H-2''), 2.39 (2H, t, *J* = 7.3 Hz, H-4''), 1.86 (2H, p, *J* = 6.9 Hz, H-3''). MS (ESI+): m/z calc. for $C_4H_7N_3O_2$ $[M+H]^+$ = 130.1; found $[M+H]^+$ = 130.1.

4-azido-*N*-(3',6'-dihydroxy-3-oxo-3*H*-spiro[isobenzofuran-1,9'-xanthen]-6-yl)butanamide (7): 4-azidobutanoic acid (**6**) (1.33 g, 8.0 mmol) was dissolved in 20 ml dichloromethane and 2.07 ml oxalyl chloride (24.0 mmol) were added to this solution. After addition of one drop of DMF, the mixture was stirred for 5 h. Evaporation of the solvents yielded the acyl chloride, which was directly used in the next step without further purification. 42 mg (crude) of 4-azidobutanoyl chloride were dissolved in 10 ml THF and dropwise added to the same amount of cooled solvent containing 0.9 equivalents of fluoresceinamine (6-isomer, 103 mg, 0.3 mmol) and 10 equivalents of $NaHCO_3$ (252 mg, 3 mmol). After complete addition of the acyl chloride, the ice bath was removed. The mixture was stirred overnight and the reaction was subsequently quenched by adding 15 ml of 5 % $NaHCO_3$ aqueous solution. The organic solvent was evaporated and the remaining solution was acidified to pH 2 by adding 5 M HCl. Ethyl acetate (3x 25 ml) was added to the suspension to extract the product from the aqueous layer. After evaporation of organic solvent, the product containing residue was purified by column chromatography using a gradient of 80-100 % ethyl acetate in cyclohexane. The desired product **7** was isolated as an orange solid. 113 mg, 82 % yield; ^{1}H NMR (400 MHz, methanol-d_4): δ 7.92 (1H, d, *J* = 8.5 Hz, H-8''), 7.76 (1H, dd, *J* = 8.4, 1.8 Hz,

H-9''), 7.58 (1H, d, *J* = 1.4 Hz, H-11''), 6.67 (2H, d, *J* = 2.4 Hz, H-17''and H-20''), 6.64 – 6.60 (2H, m, H-14'' and H-23''), 6.54 (2H, dd, *J* = 8.7, 2.4 Hz, H-15'' and H-22''), 3.36 – 3.32 (2H, m, H-2''), 2.45 (2H, t, *J* = 7.3 Hz, H-4''), 1.87 (2H, p, *J* = 6.9 Hz, H-3''). MS (ESI+): m/z calc. for $C_{24}H_{18}N_4O_6$ $[M+H]^+$ = 459.1; found $[M+H]^+$ = 459.2.

6-(2-chloroacetamido)-*N*-((1-(4-((3',6'-dihydroxy-3-oxo-3*H*-spiro[isobenzofuran-1,9'-xanthen]-6-yl)amino)-4-oxobutyl)-1*H*-1,2,3-triazol-4-yl)methyl)hexanamide (8): Method A using **4** (40 mg, 0.16 mmol) and **7 (**80 mg, 0.18 mmol). 75 mg, 66 % yield; ^{1}H NMR (400 MHz, methanol-d_4): δ 7.90 (1H, d, *J* = 8.4 Hz, H-8''), 7.81 (1H, s, H-9'), 7.70 (1H, dd, *J* = 8.4, 1.7 Hz, H-9''), 7.58 (1H, d, *J* = 1.5 Hz, H-11''), 6.67 (2H, d, *J* = 2.4 Hz, H17-'' and H-20''), 6.62 (2H, d, *J* = 8.7 Hz, H-14'' and H-23''), 6.54 (2H, dd, *J* = 8.7, 2.4 Hz, H-15'' and H-22''), 4.42 (2H, t, *J* = 6.8 Hz, H-4''), 4.35 (2H, s, H-7'), 4.00 (2H, s, NHCO-C*H*$_2$-Cl), 3.18 (2H, t, *J* = 7.1 Hz, H-6'), 2.38 (2H, t, *J* = 7.1 Hz, H-2''), 2.25 – 2.12 (4H, m, H-3'' and H2'), 1.68 – 1.43 (4H, m, H-3' and H-5'), 1.31 (2H, m, H-4'). MS (ESI+): m/z calc. for C35H35ClN6O8 $[M+Na]^+$ = 725.2105; found $[M+Na]^+$ = 725.2097.

Fl-hex-CoA (11): Method B using CoA trilithium salt (40 mg, 0.05 mmol) and **8** (42 mg, 0.06 mmol). 34 mg, 48 % yield; ^{1}H NMR (400 MHz, D_2O): δ 8.46 (1H, s, H-17), 8.13 (1H, s, H-20), 7.79 – 7.73 (2H, m, H-9' and H-8''), 7.48 (1H, dd, H-9''), 7.22 (1H, d, *J* = 2.1 Hz, H-11''), 7.07 (2H, d, *J* = 9.1 Hz, H14'' and H-23''), 6.56 – 6.49 (4H, m, H-15'', H-17'', H-20'' and H-22''), 6.08 (1H, d, *J* = 6.9 Hz, H-16), 4.97 – 4.67 (2H, m, H-14 and H-15), 4.53 – 4.47 (1H, m, H-13), 4.39 (2H, t, *J* = 6.5 Hz, H-4''), 4.22 – 4.11 (4H, m, H-12 and H-7'), 3.91 (1H, s, H7), 3.76 – 3.70 (1H, m, H-11), 3.48 – 3.42 (1H, m, H-11), 3.39 – 3.30 (2H, m, H-2), 3.18 (2H, t, *J* = 6.6 Hz, H-5), 3.06 (2H, s, H-11'), 2.98 (2H, t, *J* = 6.9 Hz, H-6'), 2.50 (2H, t, *J* = 6.7 Hz, H-1), 2.38 – 2.29 (4H, m, H-4 and H-2''), 2.20 – 2.12 (2H, m, H3''), 2.06 (2H, t, *J* = 7.3 Hz, H-2'), 1.40 (2H,, dt, *J* = 14.4, 7.2 Hz, H-5'), 1.30 (2H, dt, *J* = 15.0, 7.1 Hz, H-3'), 1.12 – 1.02 (2H, m, H4'), 0.77 (3H, s, H-9 or 10), 0.62 (3H, s, H-9 or 10).HPLC purity (HPLC-Method-B): 95.0% (t_R = 12.30 min.); HRMS (ESI$^-$): m/z calc. for $C_{56}H_{70}N_{13}O_{24}P_3S$ $[M-3H]^{3-}$ = 476.7791, $[M+Na-3H]^{2-}$ = 726.6632; found $[M-3H]^{3-}$ = 476.7790; $[M+Na-3H]^{2-}$ = 726.6630

Biotin-PEGhex-CoA (12): Method B using CoA trilithium salt (41 mg, 0.05 mmol) and **4** (15 mg, 0.06 mmol). followed by Method A using the reaction product and **10 (**45 mg, 0.06 mmol). 16 mg, 18 % yield over 2 steps; ^{1}H NMR (400 MHz, D_2O) δ 8.62 (1H, s, H-17), 8.39 (1H, s, H-20), 8.07 (1H, s, H-9'), 6.17 (1H, d, *J* = 4.7 Hz, H-16), 4.97 – 4.84 (2H, m, H-14 and H-15), 4.68 – 4.49 (4H, m, H-13, H-7'', and H-11''), 4.49 – 4.31 (3H, m, H-7' and H-9''), 4.24 (2H, s, H-12), 4.01 – 3.77 (4H, m, H-7, H-11, and H-12''), 3.67 – 3.50 (43H, m, H-11 and triazole-CH_2-CH_2-[O-CH_2-CH_2]$_{10}$-O-CH_2-CH_2-NHCO), 3.42 (2H, t, H-5), 3.36 – 3.21 (5H, m, H-2, H-6'', and H-14''), 3.19 (2H, s, H-11'), 3.11 (2H, t, *J* = 6.5 Hz, H-6'), 2.92 (1H, dd, *J* = 4.9, 13.1 Hz, H-10''), 2.70 (1H, d, *J* = 13.2 Hz, H-10''), 2.62 (2H, t, H-1), 2.42 (2H, t, H-4), 2.31 – 2.07 (4H, m, H-2' and H-2''), 1.71 – 1.16 (12H, m, H-3', H-4', H-5', H-3'', H-4'', and H-5''), 0.89 (3H, s, H-9 or 10), 0.78 (3H, s, H-9 or 10). HPLC purity (HPLC-Method B): 95.3% (t_R = 11.40 min.); HRMS (ESI$^-$): m/z calc. for $C_{66}H_{116}N_{15}O_{31}P_3S_2$ $[M+K-2H]^-$ = 1808.6102; found $[M+K-2H]^-$ = 1808.5994

Protein expression and purification:

E. coli BL21 (DE3) cells were transformed with a pQE-80L plasmid containing a 0.5 kb insert coding for the catalytic domain of human pCAF protein (bp 1923-2420 with an N-terminal His-tag). Bacteria were cultured in LB medium complemented with 100 mg/L ampicillin at 37 °C until an OD_{600} of 0.6-0.8. The recombinant expression of His-tagged pCAF catalytic domain (aa 493-658) was induced with 1 mM isopropyl-α-D-thiogalactopyranoside (IPTG) and incubated overnight at 18 °C. The cell suspension was then centrifuged and the cell pellet was resuspended in 40 ml of lysis buffer (50 mM Tris (pH 8.0), 150 mM NaCl, 1 mM β-mercaptoethanol, and 10% glycerol (v/v) with protease inhibitors (cOmplete, Mini Tablets, EDTA-free; Roche, Basel, CHE)). Cell lysis was carried out with the aid of sonification (5x 15 sec. with 1 min. pauses in between (Branson Sonifier II W-250, Heinemann, Schwäbisch Gmünd, GER)) and the resulting suspension was centrifuged (9000 rcf, 1h, 4 °C) to separate the cell debris from the soluble protein fraction. Purification of the His-tagged protein was carried out on an automated chromatography system (NGC Chromatography System, Bio-Rad Laboratories, Hercules, USA). The clear supernatant after centrifugation was filtered and loaded on a 5 ml nickel-charged IMAC column

(HisTrap HP; GE Healthcare, Chalfont St Giles, UK). After washing off non-specifically bound proteins with washing buffer (50 mM Tris (pH 8.0), 150 mM NaCl, 1 mM β-mercaptoethanol, 20 mM imidazole), a second washing step at high salt concentration (washing buffer containing 2 M NaCl and no imidazole) was included to remove residual proteins and nucleic acid contaminations. The desired protein was then eluted using 300 mM imidazole in washing buffer and the protein containing fractions were collected, pooled, and concentrated by ultrafiltration (Vivaspin® Turbo 4 concentrators, Sartorius, Göttingen, GER) to a final volume of 2 ml. Further purification of the protein solution was achieved by gel filtration on a HiLoad 26/60 Superdex 200 prep grade column (Pharmacia, New Jersey, USA) equilibrated with gel filtration buffer (22 mM Na-citrate (pH 6.5), 330 mM NaCl). Collected fractions containing the monodisperse enzyme were again pooled, concentrated by ultrafiltration, and glycerol (10% (v/v)) was added. The purity of the preparation was checked by SDS-page gel analysis and the protein concentration was determined by measuring the UV absorbance at 280 nm (Nanodrop 1000 Spectrometer, Thermo Fisher Scientific, Waltham, USA). The enzyme solution was then aliquoted, flash frozen in liquid nitrogen, and stored at -80 °C until used. *E. coli* Rosetta 2 (DE3) pLysS cells were transformed with a modified pET15b vector coding for MOF(174-449) with an N-terminal His_{10}-tag followed by a TEV protease cleavage site. Overexpression was induced in LB media at an OD of ~0.5 by the addition of IPTG (0.1 mM) and carried out at 18 °C overnight. After harvest, the bacterial pellets were resuspended in lysis buffer (50 mM HEPES, 500 mM NaCl, 20 mM imidazole, 5 mM β-mercaptoethanol, 0.01 % (w/v) taurodeoxycholate, pH 7.5) supplemented with cOmplete Mini EDTA-free protease inhibitor cocktail tablets (Roche) and lysed via sonication. After removal of cell debris, the supernatant was applied to a HisTrap HP column (1 mL, GE Healthcare, Freiburg), washed extensively with lysis buffer and then eluted with an imidazole gradient (20-300 mM). Fractions containing MOF were pooled, concentrated and purified using a HiLoad 16/60 Superdex 75 gel filtration column (GE Healthcare, Freiburg; 25 mM HEPES, 500 mM NaCl, pH 7.5). MOF-containing fractions were pooled, concentrated and flash-frozen in liquid nitrogen. All chromatography steps were performed on Äkta prime chromatography systems.

Identity of MOF was verified by mass spectrometry and protein concentration was determined using the Bradford assay.

Fluorescence Polarization Assay:

Saturation binding experiment and K_D determination: Recombinant acetyltransferase protein was serially diluted in assay buffer (50 mM HEPES (pH 7.5), 150 mM NaCl, 0.1 mM EDTA, 0.01 % BSA (w/v), 0.01 % Tween-20 (v/v) (plus 1 mM DTT in the case of p300)) to a 2x intermediate concentration. From these dilutions, 10 µl were mixed with an equal volume of a 16 nM Fl-hex-CoA solution in assay buffer on a 384-well assay plate (cat. no. 11866091, Greiner Bio-One, Kremsmünster, AUT) (20 µl final volume containing 8 nM Fl-hex-CoA and appropriate concentrations of corresponding acetyltransferase protein (0-20 µM for His-pCAF(493-658), 0-3 µM for MOF(174-449) and 0-0.75 µM for p300(1284-1673))). The plate was spun down, incubated, and measured using a 2102 EnVision® Multilabel Reader (PerkinElmer, Waltham, USA) operating in FP-mode (ex. 480 nm, em. p-plane 535 nm, em. s-plane 535 nm). All tested protein concentrations were also measured after incubation with 8 nM fluorescent probe Fl-hex-CoA in the presence of competing ligand acetonyl-CoA (200 µM final concentration), to simulate a situation, where the probe is completely displaced from the protein. In addition, the fluorescence intensities for p-plane and s-plane were measured for protein dilutions in assay buffer without Fl-hex-CoA to detect any intrinsic fluorescence not attributable to the fluorescent probe. The measured $I_{\parallel}$ and $I_{\perp}$ values were corrected for intrinsic protein fluorescence and the fluorescence polarization (P) was calculated for every protein concentration incubated with 8 nM Fl-hex-CoA in the presence (P_I) or without (P_M) competing ligand (100 µM acetonyl-CoA) using the following equation:

$$P = \frac{I_{\parallel} - G * I_{\perp}}{I_{\parallel} + G * I_{\perp}} * 1000 \ [mP]$$

In this equation, G is an instrument specific constant. The fluorescence polarization values for samples containing no protein (P_L) or the highest protein concentration (P_{L*R}), respectively resemble situations where the fluorescent probe is either free in solution or fully bound to the receptor. From these values, the fraction of bound Fl-hex-CoA (F_B) can be calculated for every protein concentration with:

$$FB = \frac{PM - PL}{PL * R - PL}$$

The contribution of non-specific binding (P_{NS}) was then determined for every protein concentration using the following equation:

$$PNS = (PI - PL) * (1 - FB)$$

The specific fluorescence polarization signals (P_S) were calculated by subtracting the non-specific portions from P_M values. The saturation binding curve was then generated by plotting P_S values against protein concentrations and the K_D value for the interaction of Fl-hex-CoA with acetyltransferase protein was calculated by fitting the corresponding results to a Hill equation using OriginPro 9 software.

Ligand evaluation: Test compounds were appropriately diluted in DMSO or H_2O to a 20x intermediate concentration. Resulting solutions were then mixed with an equal volume of assay buffer and 2 µl of the resulting dilutions were spotted into the wells of a black 384-well non-binding microplate. For positive controls (P_P), 2 µl of the solvent/assay buffer mixture without test compound were used. Next, 8 µl of a 10 nM Fl-hex-CoA solution were dispensed into each well, followed by 10 µl of acetyltransferase protein in assay buffer (P_C). Negative controls (P_N) included 10 µl of assay buffer instead of protein solution and acetonyl-CoA (50 µM final concentration) was used as a reference inhibitor. Plates were then sealed with adhesive foil (TopSeal®-A, PerkinElmer, Waltham, USA), spun down for 1 min. at 300 rcf and incubated at room temperature. Upon completion, the fluorescence intensity signals for p-plane and s-plane ($I_{//}$ and $I_{\perp}$) were read using a 2102 EnVision® Multilabel Reader (PerkinElmer, Waltham, USA) operating in FP-mode (ex. 480 nm, em. p-plane 535 nm, em. s-plane 535 nm). Results were blank corrected and the fluorescence polarization for every well was calculated as described above. Competition values (C) were calculated from the averages of controls (P_P and P_N) and determined P_C values with the use of the following equation:

$$C = \frac{(PC - PP)}{(PN - PP)} * 100 \ [\%]$$

Calculation of IC_{50} values and optical visualization were done with OriginPro 9 software by plotting competition values against logarithmic compound concentrations and applying a logistic 4 parameter sigmoidal fit with variable slope.

Biolayer Interferometry Assay:

K_D value determination for the interaction of His-pCAF(493-658) and Biotin-PEGhex-CoA: Streptavidin coated biosensors (cat. no. 18-5019, Pall FortéBio, Menlo Park, USA) were hydrated in assay buffer (50 mM HEPES (pH 7.5), 300 mM NaCl, 0.1 mM EDTA, 0.1% BSA (w/v), 0.01% Tween-20 (v/v) (plus 1 mM DTT in the case of p300)) and loaded with biotinylated probe from a 125 nM Biotin-PEGhex-CoA solution placed in the drop holder. The loaded sensor tips were then dipped into solutions of serially diluted His-pCAF(493-658) (0.04-30 µM) and the association of protein to the sensor tip was recorded for 120 sec. from the dropholder position on a BLItz® system (Pall FortéBio, Menlo Park, USA). Subsequently, the sensor tips were exposed to assay buffer and the dissociation of protein from the sensortip was recorded for 120 sec. from the tube position. A control run without enzyme was recorded for association and dissociation and the measured sample curves were referenced against this control. Global fitting of this data (for His-pCAF(493-658) concentrations spanning 0.04-3.33 µM) to a 1:1 binding model using the BLItz Pro 1.2 software gave the rate constants of association (k_a) and dissociation (k_d), as well as the affinity constant (K_D) for the interaction of His-pCAF(493-658) and Biotin-PEGhex-CoA. In a different attempt, report points of the association signal after 140 sec. total measurement time were plotted against His-pCAF(493-658) concentration and the K_D value was calculated by fitting the data to a Hill equation using OriginPro 9 software.

Ligand evaluation: To evaluate candidate ligands for competition to Biotin-PEGhex-CoA for binding to His-pCAF(493-658), compounds were appropriately diluted in DMSO or H_2O and 1 µl of each compound dilution was mixed with 19 µl acetyltransferase protein in assay buffer (final concentrations: 250 nM for His-pCAF(493-658) , 5 µM for MOF(174-449)). Positive controls received 1 µl of pure solvent (DMSO or H_2O). The mixtures were incubated for 30 min. at room temperature. At the same time, streptavidin

coated biosensors were hydrated in assay buffer and subsequently loaded with biotinylated capture ligand by exposing the sensor tips to a 125 nM solution of Biotin-PEGhex-CoA for 120 sec. in the drop holder position. After loading, a 30 sec. baseline was generated in assay buffer from the tube position. Preincubated protein solutions were then transferred to the drop holder in 4 µl volume and the association of protein to the immobilized capture ligand was measured for 120 sec. from these solutions, followed by a 120 sec. dissociation step in a tube filled with assay buffer. Recorded binding curves were referenced against a control run in assay buffer in the absence of protein. The binding signals at report points after 110 sec. of association (B_M) were used to calculate the degree of competition (C) for every ligand concentration compared to positive controls (B_P) by using the following equation:

$$C = 100 * \frac{BP - BM}{BP} \ [\%]$$

The calculated competition values were plotted against logarithmic compound concentrations and the data was fit to a four parameter logistic fit with variable slope using OriginPro 9 software.

For experiments on p300(1284-1673), 500 nM enzyme in assay buffer were incubated with 125 nM Biotin-PEGhex-CoA and appropriately diluted candidate ligands for 60 min. at room temperature in 20 µl volume. Fresh biosensor tips were hydrated and a 30 sec. baseline was recorded from assay buffer. Biosensors were then dipped into 4 µl of these mixtures and the binding signal was measured for 120 sec. from the drop holder position. Competition values were determined as described above.

Fluorescence Polarization Competition Activity Immunoassay:

Experiments were performed in assay buffer (50 mM HEPES (pH 7.5), 150 mM NaCl, 0.1 mM EDTA, 0.01 % BSA (w/v), 0.01 % Tween-20 (v/v) (+ 1 mM DTT for experiments with p300) in 25 µl final volume on black 384-well non-binding microplates (cat. no. 11866091, Greiner Bio-One, Kremsmünster, AUT). After dispensing of assay components, plates were spun down for 1 min. at 300 rcf, sealed with adhesive foil (TopSeal®-A, PerkinElmer, Waltham, USA), and incubated at room temperature. Blank controls containing 25 µl assay buffer were included in all measurements. Combinations of specific antibodies and acetylated fluorescent tracer peptides were utilized as detection reagents and the

fluorescence intensity signals of polarized light in parallel plane ($I_{//}$) and in perpendicular plane ($I_{\perp}$) with respect to the excitation light were quantified using a 2102 EnVision® Multilabel Reader (PerkinElmer, Waltham, USA) operating in FP-mode (for acH3K9-Rh: ex. 531 nm, em. p-plane 595 nm, em. s-plane 595 nm; for acH4-Fl: 480 nm, em. p-plane 535 nm, em. s-plane 535 nm).

Antibody validation: Candidate antibodies were diluted in assay buffer by the factor of 1:50. Fluorescent tracer peptides were diluted in assay buffer to 16 nM for acH3K9-Rh or 6 nM for acH4-Fl. Then, 12.5 µl of each intermediate dilution were mixed in wells of an assay plate and incubated for 30 min. at room temperature. Negative controls only received the tracer peptide and 12.5 µl of assay buffer. Blanks containing 25 µl assay buffer were also included for background correction. After incubation, the plate was spun down and FP signals were measured from all wells. The two antibodies that gave the best increase in FP signal compared to negative controls (anti-acH3K9 (cat. no. 39137, Active Motif, Carlsbad, USA) and anti-acH4 (cat. no. 177790, abcam, Cambridge, UK) were then titrated against fixed concentrations of their respective tracer peptide in 25 µl final assay volume. After 30 min. incubation, the FP values were determined and plotted against antibody concentrations.

Enzyme titration: From a serial dilution series of enzyme in assay buffer (final concentrations spanning 0-100 nM), 5 µl were mixed with 10 µl substrate (final concentrations: 50 µM H3(1-21) for pCAF(493-658), 5 µM full length H4-His for MOF(174-449) and 5 µM H4(1-23) for p300(1284-1673)) solution and 5 µl 80 µM AcCoA in assay buffer to a final volume of 20 µl in assay plates. The enzymatic reaction was allowed to proceed for 60 min. and then stopped by adding 2.5 µl of solutions containing 500 µM acetonyl-CoA and either 80 nM acH3K9-Rh or 30 nM acH4-Fl peptide. After spinning down the plate at 300 rcf and a short incubation step, 2.5 µl of antibody solution (50 µg/ml anti-acH3K9 or 4 µg/ml anti-acH4, respectively) were pipetted to each well and the plate was incubated for 30 min. at room temperature. Positive controls (P_P) received 5 µl of assay buffer instead of enzyme dilution and 2.5 µl of assay buffer instead of antibody dilution. Finally, plates were spun down at 300 rcf and the FP signals were measured from all wells. FP values measured at 0 nM enzyme concentration (P_N) were used as a negative control. The degree of competition (C) was then calculated for every enzyme concentration by

calculating the mean FP value of duplicate measurements (P_M) and inserting the values into the following equation:

$$C = \frac{(PM - PN)}{(PP - PN)} * 100\ [\%]$$

Ligand evaluation: Serial dilution series of test compounds were prepared from 10 mM stock solutions and assay buffer. 5 µl recombinant enzyme were mixed with 10 µl substrate solution and 1 µl test compound (A_I) or 1 µl assay buffer (positive control, A_P) or 1 µl of 1 mM acetonyl-CoA solution (negative control, A_N) and incubated for 5 minutes at room temperature. The enzymatic reaction was initiated by adding 4 µl of AcCoA diluted in assay buffer to the reaction mixtures. Reactions were incubated at room temperature for 60 min. with gentle shaking. Tracer peptide was diluted to a 10x intermediate concentration in assay buffer containing 1 mM acetonyl-CoA and 2.5 µl of this mixture was added to every reaction and control wells followed by 2.5 µl of a 10x concentrated antibody dilution, after a short incubation step. The plates were spun down, incubated for 30 min. at room temperature and FP signals were measured as described above. Inhibition values (I) were calculated from the averages of controls (A_P and A_N) and measured A_I values with the use of the following equation:

$$I = \frac{(AI - AP)}{(AN - AP)} * 100\ [\%]$$

Calculation of IC_{50} values were done with OriginPro 9 software by plotting inhibition values against logarithmic compound concentrations and applying a logistic 4 parameter sigmoidal fit with variable slope.

ANCILLARY INFORMATION

Supporting Information.

Supporting information is available free of charge via the Internet at http://pubs.acs.org.

- HPLC chromatograms and NMR spectra of reference inhibitor acetonyl-CoA and compounds **11**, and **12**.
- Information on atom numbering and used peptides.
- Supplemental methods and additional figures illustrating probe validation, ITC measurements, FP, BLI, and activity assay optimization and compound profiling.
- Supplemental references.
- Molecular Formular Strings (CSV)

AUTHOR INFORMATION

Corresponding Author

*Phone: +497612034896. Fax: +497612036321. E-mail: manfred.jung@pharmazie.uni-freiburg.de.

Funding Sources

This work was funded by the Deutsche Forschungsgemeinschaft (DFG) - SPP 1463, 235777276/GRK1976, and SFB992.

Notes

The authors declare no competing financial interest.

ACKNOWLEDGMENT

We thank Marie Markones and Prof. Heiko Heerklotz, University of Freiburg, Germany, for their help with ITC data collection and Marcel Wilde, Jan-Patrick Steitz and Prof. Michael Müller, University of Freiburg, Germany, for their help with pCAF expression and purification. We further acknowledge Sascha Ferlaino and the MagRes unit for NMR measurements.

ABBREVIATIONS

Ab, antibody; Alpha, amplified luminescent proximity homogeneous assay; BLI, biolayer interferometry; DIPEA, N,N-diisopropylethylamine; Fl, fluorescein; FP, fluorescence polarization; HBTU, 3-[Bis(dimethylamino)methyliumyl]-3*H*-benzotriazol-1-oxide hexafluorophosphate; ITC, isothermal titration calorimetry; K_D, dissociation constant; MOF, male absent on the first; pCAF, p300/CBP associated factor; rcf, relative centrifugal force; Rh, rhodanin; SEM, standard error of the mean; TBTA, Tris[(1-benzyl-1H-1,2,3-triazol-4-yl)methyl]amine; TEAB, triethylammonium bicarbonate

REFERENCES

1. Choudhary, C.; Kumar, C.; Gnad, F.; Nielsen, M. L.; Rehman, M.; Walther, T. C.; Olsen, J. V.; Mann, M., Lysine Acetylation Targets Protein Complexes and Co-Regulates Major Cellular Functions. *Science* **2009,** *325* (5942), 834-840.

2. Zhao, S.; Xu, W.; Jiang, W.; Yu, W.; Lin, Y.; Zhang, T.; Yao, J.; Zhou, L.; Zeng, Y.; Li, H.; Li, Y.; Shi, J.; An, W.; Hancock, S. M.; He, F.; Qin, L.; Chin, J.; Yang, P.; Chen, X.; Lei, Q.; Xiong, Y.; Guan, K. L., Regulation of Cellular Metabolism by Protein Lysine Acetylation. *Science* **2010,** *327* (5968), 1000-1004.

3. Ali, I.; Conrad, R. J.; Verdin, E.; Ott, M., Lysine Acetylation Goes Global: From Epigenetics to Metabolism and Therapeutics. *Chem. Rev.* **2018,** *118* (3), 1216-1252.

4. Kim, S. C.; Sprung, R.; Chen, Y.; Xu, Y.; Ball, H.; Pei, J.; Cheng, T.; Kho, Y.; Xiao, H.; Xiao, L.; Grishin, N. V.; White, M.; Yang, X. J.; Zhao, Y., Substrate and Functional Diversity of Lysine Acetylation Revealed by a Proteomics Survey. *Mol. Cell* **2006,** *23* (4), 607-618.

5. Leemhuis, H.; Packman, L. C.; Nightingale, K. P.; Hollfelder, F., The Human Histone Acetyltransferase P/Caf Is a Promiscuous Histone Propionyltransferase. *Chembiochem* **2008,** *9* (4), 499-503.

6. Han, Z.; Wu, H.; Kim, S.; Yang, X.; Li, Q.; Huang, H.; Cai, H.; Bartlett, M. G.; Dong, A.; Zeng, H.; Brown, P. J.; Yang, X. J.; Arrowsmith, C. H.; Zhao, Y.; Zheng, Y. G., Revealing the Protein

Propionylation Activity of the Histone Acetyltransferase Mof (Males Absent on the First). *J. Biol. Chem.* **2018,** *293* (9), 3410-3420.

7. Chen, Y.; Sprung, R.; Tang, Y.; Ball, H.; Sangras, B.; Kim, S. C.; Falck, J. R.; Peng, J.; Gu, W.; Zhao, Y., Lysine Propionylation and Butyrylation Are Novel Post-Translational Modifications in Histones. *Mol. Cell. Proteomics* **2007,** *6* (5), 812-819.

8. Brownell, J. E.; Allis, C. D., An Activity Gel Assay Detects a Single, Catalytically Active Histone Acetyltransferase Subunit in Tetrahymena Macronuclei. *Proc. Natl. Acad. Sci. U. S. A.* **1995,** *92* (14), 6364-6368.

9. Yang, X. J.; Ogryzko, V. V.; Nishikawa, J.; Howard, B. H.; Nakatani, Y., A P300/Cbp-Associated Factor That Competes with the Adenoviral Oncoprotein E1a. *Nature* **1996,** *382* (6589), 319-324.

10. Parthun, M. R.; Widom, J.; Gottschling, D. E., The Major Cytoplasmic Histone Acetyltransferase in Yeast: Links to Chromatin Replication and Histone Metabolism. *Cell* **1996,** *87* (1), 85-94.

11. Friedmann, D. R.; Aguilar, A.; Fan, J.; Nachury, M. V.; Marmorstein, R., Structure of the Alpha-Tubulin Acetyltransferase, Alphatat1, and Implications for Tubulin-Specific Acetylation. *Proc. Natl. Acad. Sci. U. S. A.* **2012,** *109* (48), 19655-19660.

12. Whyte, P.; Williamson, N. M.; Harlow, E., Cellular Targets for Transformation by the Adenovirus E1a Proteins. *Cell* **1989,** *56* (1), 67-75.

13. Chrivia, J. C.; Kwok, R. P.; Lamb, N.; Hagiwara, M.; Montminy, M. R.; Goodman, R. H., Phosphorylated Creb Binds Specifically to the Nuclear Protein Cbp. *Nature* **1993,** *365* (6449), 855-859.

14. Smith, E. R.; Pannuti, A.; Gu, W.; Steurnagel, A.; Cook, R. G.; Allis, C. D.; Lucchesi, J. C., The Drosophila Msl Complex Acetylates Histone H4 at Lysine 16, a Chromatin Modification Linked to Dosage Compensation. *Mol. Cell. Biol.* **2000,** *20* (1), 312-318.

15. Allis, C. D.; Berger, S. L.; Cote, J.; Dent, S.; Jenuwein, T.; Kouzarides, T.; Pillus, L.; Reinberg, D.; Shi, Y.; Shiekhattar, R.; Shilatifard, A.; Workman, J.; Zhang, Y., New Nomenclature for Chromatin-Modifying Enzymes. *Cell* **2007,** *131* (4), 633-636.

16. Sapountzi, V.; Logan, I. R.; Robson, C. N., Cellular Functions of Tip60. *Int. J. Biochem. Cell Biol.* **2006,** *38* (9), 1496-1509.

17. Iizuka, M.; Stillman, B., Histone Acetyltransferase Hbo1 Interacts with the Orc1 Subunit of the Human Initiator Protein. *J. Biol. Chem.* **1999,** *274* (33), 23027-23034.

18. Karmodiya, K.; Anamika, K.; Muley, V.; Pradhan, S. J.; Bhide, Y.; Galande, S., Camello, a Novel Family of Histone Acetyltransferases That Acetylate Histone H4 and Is Essential for Zebrafish Development. *Sci. Rep.* **2014,** *4*, 6076.

19. Doi, M.; Hirayama, J.; Sassone-Corsi, P., Circadian Regulator Clock Is a Histone Acetyltransferase. *Cell* **2006,** *125* (3), 497-508.

20. Chen, H.; Lin, R. J.; Schiltz, R. L.; Chakravarti, D.; Nash, A.; Nagy, L.; Privalsky, M. L.; Nakatani, Y.; Evans, R. M., Nuclear Receptor Coactivator Actr Is a Novel Histone Acetyltransferase and Forms a Multimeric Activation Complex with P/Caf and Cbp/P300. *Cell* **1997,** *90* (3), 569-580.

21. Hou, F.; Zou, H., Two Human Orthologues of Eco1/Ctf7 Acetyltransferases Are Both Required for Proper Sister-Chromatid Cohesion. *Mol. Biol. Cell* **2005,** *16* (8), 3908-3918.

22. Lin, H.; Su, X.; He, B., Protein Lysine Acylation and Cysteine Succination by Intermediates of Energy Metabolism. *ACS Chem. Biol.* **2012,** *7* (6), 947-960.

23. Schneider, A.; Chatterjee, S.; Bousiges, O.; Selvi, B. R.; Swaminathan, A.; Cassel, R.; Blanc, F.; Kundu, T. K.; Boutillier, A. L., Acetyltransferases (Hats) as Targets for Neurological Therapeutics. *Neurotherapeutics* **2013,** *10* (4), 568-588.

24. Cereseto, A.; Manganaro, L.; Gutierrez, M. I.; Terreni, M.; Fittipaldi, A.; Lusic, M.; Marcello, A.; Giacca, M., Acetylation of Hiv-1 Integrase by P300 Regulates Viral Integration. *EMBO J.* **2005,** *24* (17), 3070-3081.

25. Carneiro, V. C.; de Abreu da Silva, I. C.; Torres, E. J.; Caby, S.; Lancelot, J.; Vanderstraete, M.; Furdas, S. D.; Jung, M.; Pierce, R. J.; Fantappie, M. R., Epigenetic Changes Modulate Schistosome Egg Formation and Are a Novel Target for Reducing Transmission of Schistosomiasis. *PLoS Pathog.* **2014,** *10* (5), e1004116.

26. Dekker, F. J.; van den Bosch, T.; Martin, N. I., Small Molecule Inhibitors of Histone Acetyltransferases and Deacetylases Are Potential Drugs for Inflammatory Diseases. *Drug Discovery Today* **2014,** *19* (5), 654-660.

27. Bandyopadhyay, D.; Okan, N. A.; Bales, E.; Nascimento, L.; Cole, P. A.; Medrano, E. E., Down-Regulation of P300/Cbp Histone Acetyltransferase Activates a Senescence Checkpoint in Human Melanocytes. *Cancer Res.* **2002,** *62* (21), 6231-6239.

28. Heery, D. M.; Fischer, P. M., Pharmacological Targeting of Lysine Acetyltransferases in Human Disease: A Progress Report. *Drug Discovery Today* **2007,** *12* (1-2), 88-99.

29. Sun, X. J.; Wang, Z.; Wang, L.; Jiang, Y.; Kost, N.; Soong, T. D.; Chen, W. Y.; Tang, Z.; Nakadai, T.; Elemento, O.; Fischle, W.; Melnick, A.; Patel, D. J.; Nimer, S. D.; Roeder, R. G., A Stable Transcription Factor Complex Nucleated by Oligomeric Aml1-Eto Controls Leukaemogenesis. *Nature* **2013,** *500* (7460), 93-97.

30. Chen, S.; Feng, B.; George, B.; Chakrabarti, R.; Chen, M.; Chakrabarti, S., Transcriptional Coactivator P300 Regulates Glucose-Induced Gene Expression in Endothelial Cells. *Am. J. Physiol. Endocrinol. Metab.* **2010,** *298* (1), E127-E137.

31. Lee, K. K.; Workman, J. L., Histone Acetyltransferase Complexes: One Size Doesn't Fit All. *Nat. Rev. Mol. Cell Biol.* **2007,** *8* (4), 284-295.

32. Lasko, L. M.; Jakob, C. G.; Edalji, R. P.; Qiu, W.; Montgomery, D.; Digiammarino, E. L.; Hansen, T. M.; Risi, R. M.; Frey, R.; Manaves, V.; Shaw, B.; Algire, M.; Hessler, P.; Lam, L. T.; Uziel, T.; Faivre, E.; Ferguson, D.; Buchanan, F. G.; Martin, R. L.; Torrent, M.; Chiang, G. G.; Karukurichi, K.; Langston, J. W.; Weinert, B. T.; Choudhary, C.; de Vries, P.; Van Drie, J. H.; McElligott, D.; Kesicki, E.; Marmorstein, R.; Sun, C.; Cole, P. A.; Rosenberg, S. H.; Michaelides, M. R.; Lai, A.; Bromberg, K. D., Discovery of a Selective Catalytic P300/Cbp Inhibitor That Targets Lineage-Specific Tumours. *Nature* **2017,** *550* (7674), 128-132.

33. Baell, J. B.; Leaver, D. J.; Hermans, S. J.; Kelly, G. L.; Brennan, M. S.; Downer, N. L.; Nguyen, N.; Wichmann, J.; McRae, H. M.; Yang, Y.; Cleary, B.; Lagiakos, H. R.; Mieruszynski, S.; Pacini, G.;

Vanyai, H. K.; Bergamasco, M. I.; May, R. E.; Davey, B. K.; Morgan, K. J.; Sealey, A. J.; Wang, B.; Zamudio, N.; Wilcox, S.; Garnham, A. L.; Sheikh, B. N.; Aubrey, B. J.; Doggett, K.; Chung, M. C.; de Silva, M.; Bentley, J.; Pilling, P.; Hattarki, M.; Dolezal, O.; Dennis, M. L.; Falk, H.; Ren, B.; Charman, S. A.; White, K. L.; Rautela, J.; Newbold, A.; Hawkins, E. D.; Johnstone, R. W.; Huntington, N. D.; Peat, T. S.; Heath, J. K.; Strasser, A.; Parker, M. W.; Smyth, G. K.; Street, I. P.; Monahan, B. J.; Voss, A. K.; Thomas, T., Inhibitors of Histone Acetyltransferases Kat6a/B Induce Senescence and Arrest Tumour Growth. *Nature* **2018,** *560* (7717), 253-257.

34. Simon, R. P.; Robaa, D.; Alhalabi, Z.; Sippl, W.; Jung, M., Katching-up on Small Molecule Modulators of Lysine Acetyltransferases. *J. Med. Chem.* **2016,** *59* (4), 1249-1270.

35. Dahlin, J. L.; Nelson, K. M.; Strasser, J. M.; Barsyte-Lovejoy, D.; Szewczyk, M. M.; Organ, S.; Cuellar, M.; Singh, G.; Shrimp, J. H.; Nguyen, N.; Meier, J. L.; Arrowsmith, C. H.; Brown, P. J.; Baell, J. B.; Walters, M. A., Assay Interference and Off-Target Liabilities of Reported Histone Acetyltransferase Inhibitors. *Nat. Commun.* **2017,** *8* (1), 1527.

36. Lau, O. D.; Kundu, T. K.; Soccio, R. E.; Ait-Si-Ali, S.; Khalil, E. M.; Vassilev, A.; Wolffe, A. P.; Nakatani, Y.; Roeder, R. G.; Cole, P. A., Hats Off: Selective Synthetic Inhibitors of the Histone Acetyltransferases P300 and Pcaf. *Mol. Cell* **2000,** *5* (3), 589-595.

37. Rubenstein, P.; Dryer, R., S-Acetonyl-Coa. A Nonreactive Analog of Acetyl-Coa. *J. Biol. Chem.* **1980,** *255* (16), 7858-7862.

38. He, M.; Han, Z.; Liu, L.; Zheng, Y. G., Chemical Biology Approaches for Investigating the Functions of Lysine Acetyltransferases. *Angew. Chem., Int. Ed. Engl.* **2018,** *57* (5), 1162-1184.

39. Hwang, Y.; Thompson, P. R.; Wang, L.; Jiang, L.; Kelleher, N. L.; Cole, P. A., A Selective Chemical Probe for Coenzyme a-Requiring Enzymes. *Angew. Chem., Int. Ed.* **2007,** *46* (40), 7621-7624.

40. Han, Z.; Chou, C. W.; Yang, X.; Bartlett, M. G.; Zheng, Y. G., Profiling Cellular Substrates of Lysine Acetyltransferases Gcn5 and P300 with Orthogonal Labeling and Click Chemistry. *ACS Chem. Biol.* **2017,** *12* (6), 1547-1555.

41. Yang, C.; Mi, J.; Feng, Y.; Ngo, L.; Gao, T.; Yan, L.; Zheng, Y. G., Labeling Lysine Acetyltransferase Substrates with Engineered Enzymes and Functionalized Cofactor Surrogates. *J. Am. Chem. Soc.* **2013,** *135* (21), 7791-7794.

42. Montgomery, D. C.; Sorum, A. W.; Guasch, L.; Nicklaus, M. C.; Meier, J. L., Metabolic Regulation of Histone Acetyltransferases by Endogenous Acyl-Coa Cofactors. *Chem. Biol.* **2015,** *22* (8), 1030-1039.

43. Tanner, K. G.; Langer, M. R.; Denu, J. M., Kinetic Mechanism of Human Histone Acetyltransferase P/Caf. *Biochemistry* **2000,** *39* (50), 15652.

44. Wapenaar, H.; van der Wouden, P. E.; Groves, M. R.; Rotili, D.; Mai, A.; Dekker, F. J., Enzyme Kinetics and Inhibition of Histone Acetyltransferase Kat8. *Eur. J. Med. Chem.* **2015,** *105*, 289-296.

45. Kaczmarska, Z.; Ortega, E.; Goudarzi, A.; Huang, H.; Kim, S.; Marquez, J. A.; Zhao, Y.; Khochbin, S.; Panne, D., Structure of P300 in Complex with Acyl-Coa Variants. *Nat. Chem. Biol.* **2017,** *13* (1), 21-29.

46. Montgomery, D. C.; Garlick, J. M.; Kulkarni, R. A.; Kennedy, S.; Allali-Hassani, A.; Kuo, Y. M.; Andrews, A. J.; Wu, H.; Vedadi, M.; Meier, J. L., Global Profiling of Acetyltransferase Feedback Regulation. *J Am Chem Soc* **2016,** *138* (20), 6388-6391.

47. Zhang, J. H.; Chung, T. D.; Oldenburg, K. R., A Simple Statistical Parameter for Use in Evaluation and Validation of High Throughput Screening Assays. *J Biomol Screen* **1999,** *4* (2), 67-73.

48. Seethala, R.; Menzel, R., A Fluorescence Polarization Competition Immunoassay for Tyrosine Kinases. *Anal. Biochem.* **1998,** *255* (2), 257-262.

49. Cheng, Y.; Prusoff, W. H., Relationship between the Inhibition Constant (K1) and the Concentration of Inhibitor Which Causes 50 Per Cent Inhibition (I50) of an Enzymatic Reaction. *Biochem. Pharmacol.* **1973,** *22* (23), 3099-3108.

50. Ringel, A. E.; Wolberger, C., Structural Basis for Acyl-Group Discrimination by Human Gcn5l2. *Acta Crystallogr. D Struct. Biol.* **2016,** *72* (7), 841-848.

51. Clements, A.; Rojas, J. R.; Trievel, R. C.; Wang, L.; Berger, S. L.; Marmorstein, R., Crystal Structure of the Histone Acetyltransferase Domain of the Human Pcaf Transcriptional Regulator Bound to Coenzyme A. *EMBO J.* **1999,** *18* (13), 3521-3532.

52. Liu, X.; Wang, L.; Zhao, K.; Thompson, P. R.; Hwang, Y.; Marmorstein, R.; Cole, P. A., The Structural Basis of Protein Acetylation by the P300/Cbp Transcriptional Coactivator. *Nature* **2008,** *451* (7180), 846-850.

53. Kadlec, J.; Hallacli, E.; Lipp, M.; Holz, H.; Sanchez-Weatherby, J.; Cusack, S.; Akhtar, A., Structural Basis for Mof and Msl3 Recruitment into the Dosage Compensation Complex by Msl1. *Nat. Struct. Mol. Biol.* **2011,** *18* (2), 142-149.

54. Cebrat, M.; Kim, C. M.; Thompson, P. R.; Daugherty, M.; Cole, P. A., Synthesis and Analysis of Potential Prodrugs of Coenzyme a Analogues for the Inhibition of the Histone Acetyltransferase P300. *Bioorg. Med. Chem.* **2003,** *11* (15), 3307-3313.

55. Hwang, Y.; Ganguly, S.; Ho, A. K.; Klein, D. C.; Cole, P. A., Enzymatic and Cellular Study of a Serotonin N-Acetyltransferase Phosphopantetheine-Based Prodrug. *Bioorg. Med. Chem.* **2007,** *15* (5), 2147-2155.

56. Price, A. J.; Howard, S.; Cons, B. D., Fragment-Based Drug Discovery and Its Application to Challenging Drug Targets. *Essays Biochem.* **2017,** *61* (5), 475-484.

TABLES

Table 1. pCAF-binding constants determined for the reference inhibitor acetonyl-CoA and the probes.

Method	K_D (IC_{50}) ± SD [μM]		
	acetonyl-CoA	Fl-hex-CoA (11)	Biotin-PEGhex-CoA (12)
ITC	0.71 ± 0.31	0.75 ± 0.36	1.39 ± 0.23
BLI[a]	(0.78 ± 0.10)	(0.98 ± 0.10)	1.00 ± 0.28
FP	0.59 ± 0.07	0.82 ± 0.03	0.71 ± 0.08

[a] Values determined by BLI in the competition binding experiment were not recalculated to K_D values, but reported as the measured IC_{50} in parenthesis.

Table 2. Results from FP competition activity immonoassay optimization.

	enzyme conc. [nM]	substrate (conc. [μM])	AcCoA conc. (K_m) [μM]	K_i ref. inhib. ± SD [μM]	Z'-factor
His-pCAF$_{(493-658)}$	30	H3(1-21) (50)	6 (2.6)	1.32 ± 0.42	0.56
MOF$_{(174-449)}$	50	H4-His (5)	10 (5.6)	2.83 ± 0.61	0.78
p300$_{(1284-1673)}$	15	H4(1-23) (5)	4 (1.3)	0.88 ± 0.14	0.79

Table 3. FP assay results from acyl-CoA profiling.

	K_D (IC_{50}) ± SD [μM]	
	pCAF(493-658)	p300(1284-1673)
CoA-SH	9.01 ± 2.86	5.45 ± 0.57
AcCoA	1.03 ± 0.16	0.64 ± 0.09
butyryl-CoA	7.05 ± 0.66	0.38 ± 0.10
lauroyl-CoA	0.18 ± 0.02	(0.08 ± 0.02)[b]

[b] The IC_{50} of lauroyl-CoA for p300 in the FP assay is too low to reliably calculate the affinity constant. Therefore, the IC_{50} is reported here.

FIGURE LEGENDS

Figure 1. General structures of selected CoA-derived metabolites, KAT inhibitors, and chemical probes.

Figure 2. Structures of new functionally labelled cofactor analogues 11 and 12 from this study. Labels are colored in orange and lysine mimicking linkers are depicted in blue.

Figure 3. Schematic depictions of the FP and the BLI assay and response plots of pCAF(493-658) within these assay systems. a) Setup of the FP assay. The FP signal is dependent on the rotational freedom of the fluorescent tracer, which is influenced by the presence of competing ligands. b) Saturation binding curve of pCAF(493-658) binding to 8 nM of **11** and dose-response curve of reference inhibitor acetonyl-CoA against 400 nM pCAF and 8 nM **11** after different time points. Data represent the mean and standard deviation of triplicate measurements. c) Setup of the BLI assay. Compound **12** was immobilized on streptavidin coated sensors and the association and dissociation of enzyme in the presence of possible competitors is monitored by measuring the optical interference pattern of two light beams within the sensor. d) Sensorgrams and saturation binding curve of a concentration series of pCAF(493-658) in the BLI assay. e) Sensorgrams and dose-response curve of the reference inhibitor titration against 250 nM enzyme. Data represents the mean and standard deviation of triplicate measurements. Results are summarized in Table 1.

Figure 4. Results from the method transfer to other KATs. a) Titration curves of p300(1284-1673) and MOF(174-449) against 8 nM **11** and dose-response curves of reference inhibitor against both enzymes at optimized assay concentrations of 120 nM and 800 nM, respectively. b) Sensorgrams and corresponding dose-response curves from BLI experiments measuring the concentration dependent competition of

acetonyl-CoA with p300(1284-1673) and MOF(174-449) for binding to immobilized **12**. Data represent the mean and standard deviation of duplicate measurements

Figure 5. Results from antibody and enzyme titrations. a) Titration curves of anti-acH4-Ab and anti-acH3K9-Ab against 3 nM acH4-Fl and 8 nM acH3K9-Rh tracer peptide, respectively, after 30 min incubation. b) Concentration-response curves for acetyltransferases after 60 min incubation with substrate (50 μM H3(1-21) for pCAF(493-658), 5 μM full length H4-His for MOF(174-449), 5 μM H4(1-23) for p300(1284-1673)) and 20 μM AcCoA. The degree of competition was measured after stopping the reaction by addition of the corresponding tracer/antibody pair. Data represent the mean and standard deviation of triplicate measurements.

Figure 6. Results from acyl-CoA profiling and binding site mapping. a) Comparison of FP and BLI assay results from acyl-CoA profiling against pCAF(493-658). b) Thermal shift profiles of acyl-CoAs interacting with 4 μM pCAF(493-658). The melting temperature shifts compared to apo-pCAF are depicted in the insertion. c) Dose-response curves for acyl-CoA variants in the FP assay (top: pCAF(493-658); bottom: p300(1284-1673)). The curves for butyryl-CoA are depicted in red. d) Dose-response curves of lauroyl-CoA (solid lines) and reference inhibitor acetonyl-CoA (dashed lines) in the FP competition activity immunoassay for p300 (orange) and pCAF (green). e) Competition profiles of cofactor fragments against all three KAT enzymes in the FP assay. All data represent the mean and standard deviation of triplicate (pCAF) or duplicate (p300 and MOF) measurements.

Figure 7. Results from ligand screening. a) Bar graph and cumulative distribution of the primary screening. The threshold was set to 2 x SD (σ) over all measurements. b) Thermal shifts of screening hits at 1 mM compound concentrations. Destabilizing compounds were sorted out. c) BLI sensorgrams of hits from the confirmatory assay. d) Structures of the three fragment screening hits.

SCHEME LEGENDS

Scheme 1. Synthesis of cofactor-based probes. *Reagents and conditions* (a): propargylamine, HBTU, DIPEA, DCM, rt, overnight; (b): TFA/DCM 1:1, 1h then chloroacetyl chloride, DMF, 0 °C to rt, 1 h; (c): 1*H*-imidazole-1-sulfonyl azide*HCl, $CuSO_4$, K_2CO_3, MeOH, rt, overnight; (d): 1. $(COCl)_2$, cat. DMF, DCM, rt, 5h; 2. 6-aminofluorescein, $NaHCO_3$, THF, rt, overnight; (e): Coenzyme A, 20% ethanol in 0.1 M TEAB buffer pH 8, 0 °C to rt, 2 h; (f): alkyl azide, TBTA, $CuSO_4$, sodium ascorbate, *tert*-BuOH/H_2O/DMF (1:1:1), rt, 12 h. DIPEA = *N,N*-diisopropylethylamine, rt = room temperature, TEAB = triethylammonium bicarbonate, TBTA = Tris[(1-benzyl-1*H*-1,2,3-triazol-4-yl)methyl]amine.

Scheme 2. Schematic depiction of the FP competition activity immunoassay. Substrate peptide is processed by the acetyltransferase in the course of the enzymatic reaction. After incubation, the reaction is stopped by addition of reference inhibitor and the tracer/receptor pair is added. Acetylated reaction product competes with a fluorescence labelled peptide (tracer) for binding to the modification specific antibody (receptor). The decrease in fluorescence polarization of the tracer peptide is proportional to its displacement from the antibody and therefore a measure for enzymatic turnover.

FIGURES

Figure 1.

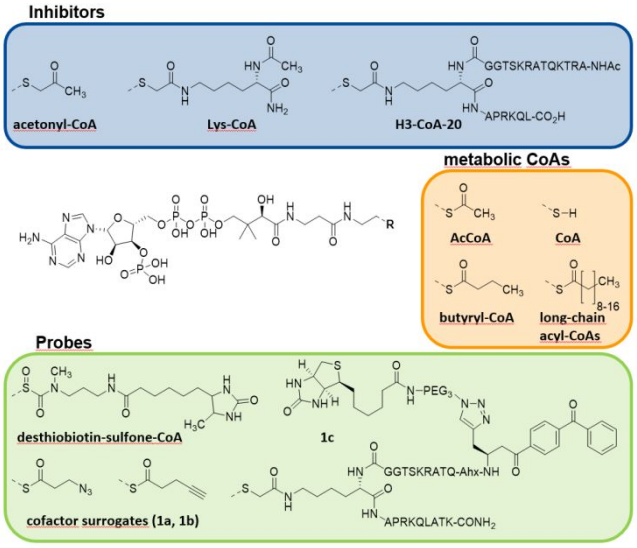

Figure 2.

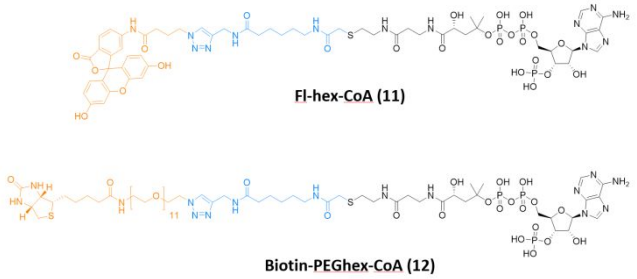

Figure 3.

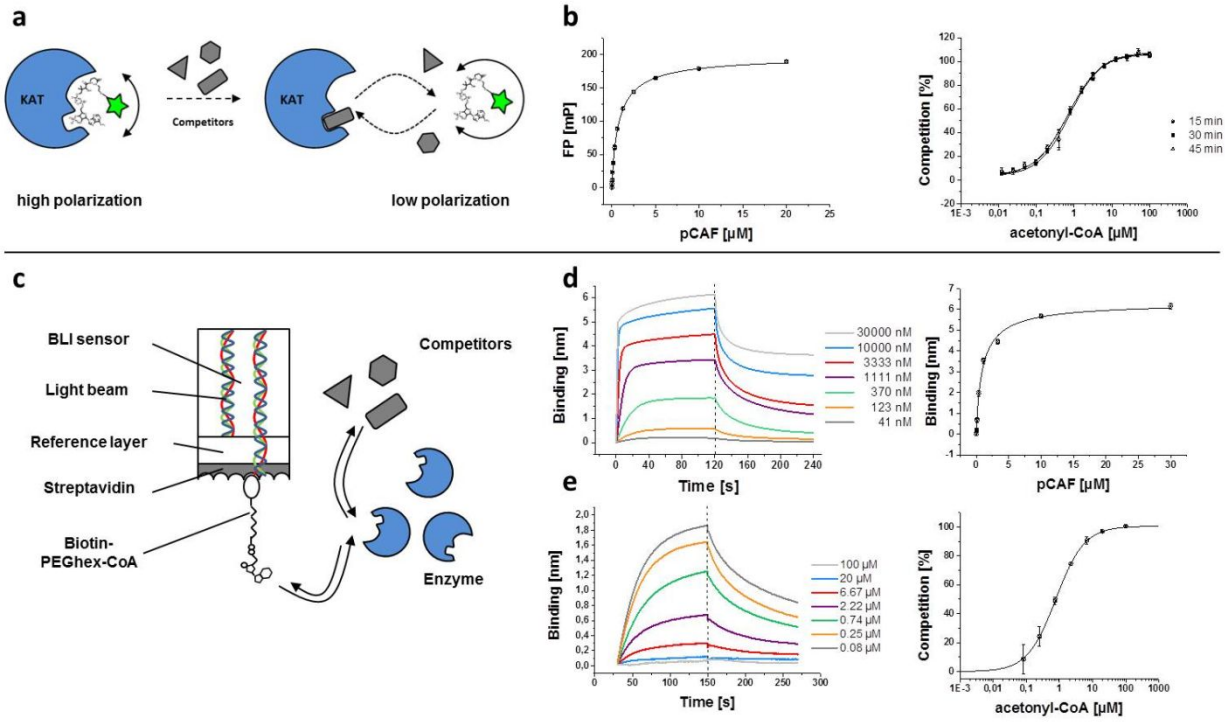

Figure 4.

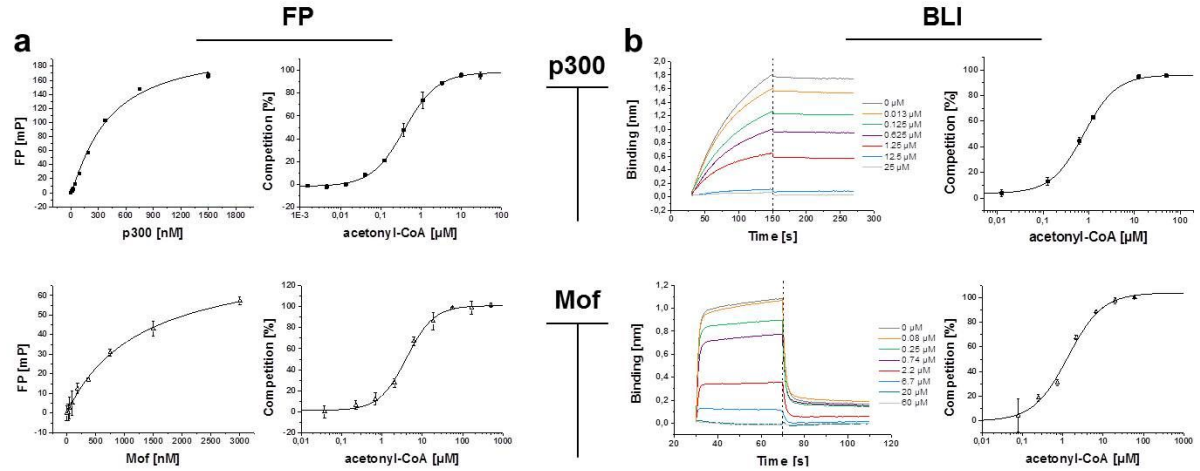

Figure 5.

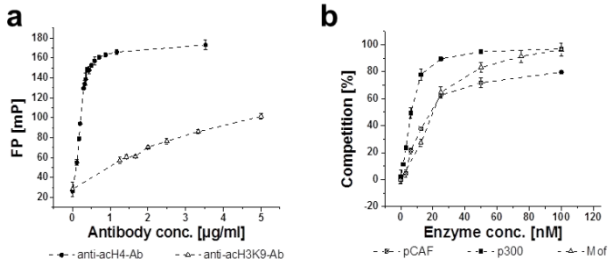

Figure 6.

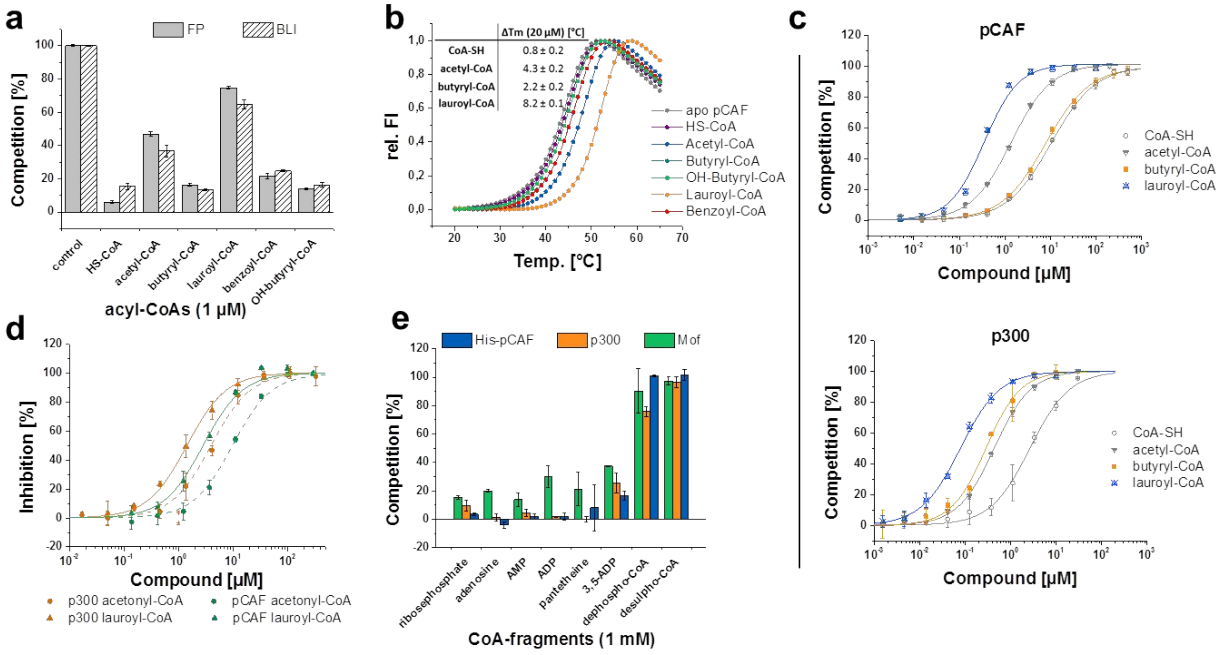

Figure 7.

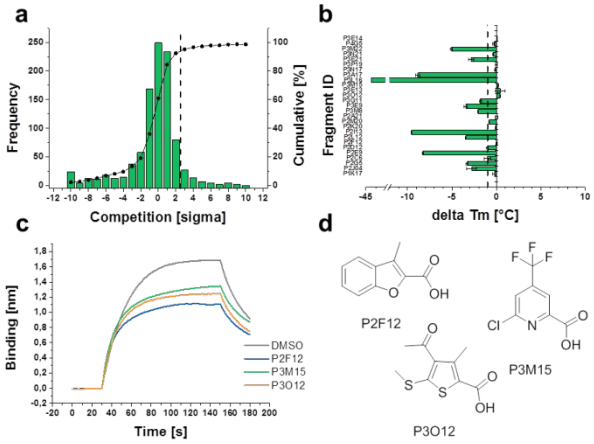
a
Frequency
Cumulative [%]
Competition [sigma]
b
Fragment ID
delta Tm [°C]
c
Binding [nm]
Time [s]
DMSO
P2F12
P3M15
P3O12
d
P2F12
P3M15
P3O12

SCHEMES

Scheme 1.

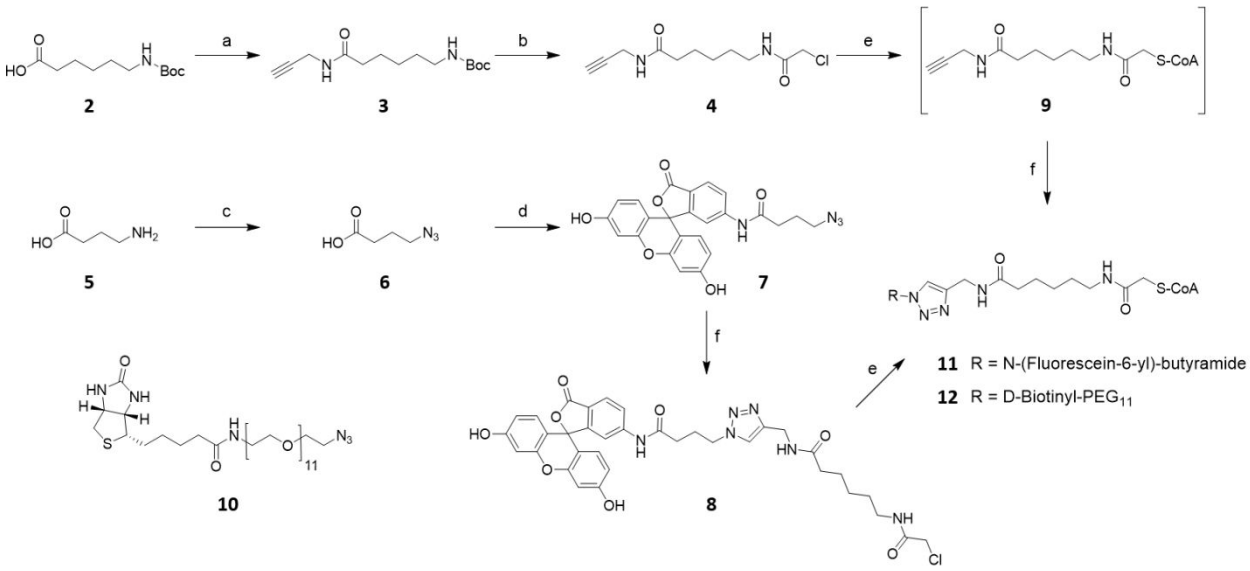

Scheme 2.

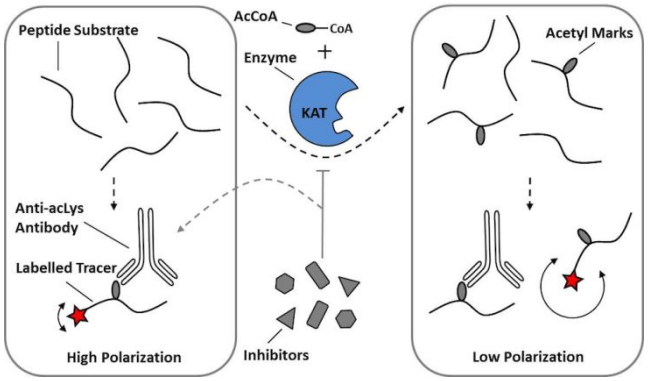

TABEL OF CONTENTS GRAPHIC